Theses and Dissertations   Graduate School

2009

EXPERIMENTAL AND NUMERICAL INVESTIGATION ON PYROELECTRIC ENERGY SCAVENGING

Jingsi Xie
Virginia Commonwealth University

EXPERIMENTAL AND NUMERICAL INVESTIGATION ON PYROELECTRIC

ENERGY SCAVENGING

A thesis submitted in partial fulfillment of the requirements for the degree of Master of Science at Virginia Commonwealth University.

by

JINGSI XIE
Electrical Engineering,
Southwest Jiaotong University, July 6th, Chengdu, P.R. China, 2007

Director: DR. KARLA MOSSI
ASSOCIATE PROFESSOR, MECHANICAL ENGINEERING

Virginia Commonwealth University
Richmond, Virginia
May, 2010

Acknowledgement

I would like to express my sincere gratitude to the people who provided invaluable encourage and help to me during my first two years life in US.

Foremost, I would like to thank my advisor Dr. Karla Mossi for her advice, guidance, encouragement and continuous support during my graduate study and research. Without her help, this work would not be possible. I could not have imagined having a better advisor and mentor for my graduate study.

Besides my advisor, I would like to thank the rest of my thesis committee: Dr. Leang, Dr. Atulasimha and Dr. Atkinson, who took time out of their busy schedules to be a part of my committee. Your suggestions were most useful and helped me understanding the concepts better.

I would like to thank my fellow labmates in Smart Materials Lab. A special thanks to Dr. Poorna Mane for the help she provided when I was new here, for the time we were working together, for all the fun we have had in the pasting time.

Last but not the least, I would like to thank my family especially my dear parents, for giving birth to me at the first place and supporting me spiritually throughout my life. It is the everlasting loves from them to my whole life that creates my tomorrow.

Table of Contents

List of Tables

List of Figures

Abstract

EXPERIMENTAL AND NUMERICAL INVESTIGATION ON PYROELECTRIC

ENERGY SCAVENGING

By Jingsi Xie, B.S.

A thesis submitted in partial fulfillment of the requirements for the degree of Master of Science in Engineering at Virginia Commonwealth University.

Virginia Commonwealth University, 2009

Major Director: Dr. Karla Mossi
Associate Professor, Mechanical Engineering

Pyroelectric energy scavenging is the process of converting wasted energy from a system to power another one, based on the pyroelectric effect of piezoelectric materials. Pyroelectrically generated power is a function of the surface of material, the pyroelectric coefficient, and the temporal temperature gradient. In the current project, a simple model is developed to predict the power generation based on the temporal change in temperature of material. In addition, a model is validated with experimental measurements from several piezoelectric materials. It is shown that energy generation can be enhanced by using piezoelectric materials with significantly higher pyroelectric coefficients such as pre-stressed piezoelectric materials or thin films. Meanwhile, a method of continuously

harvesting energy from pyroelectric materials is demonstrated using an innovative cyclic heating scheme. The proposed method uses radiation heating and natural cooling such that at smaller cyclic frequencies the temperature gradients are larger and thus higher power densities. For static heating system, the measured results were in good agreement with the predicted results for the PMN-PT, PVDF and PZT-5A, which were within 4%, 8% and 9%. Peak power densities were experimentally determined to be $0.33\mu\text{Wcm}^{-2}$, $0.20\mu\text{Wcm}^{-2}$, and $0.12\mu\text{Wcm}^{-2}$, for PMN-PT, PVDF, and PZT-5A, respectively. The predicted peak power density under similar boundary conditions for thin-film lead scandium tantalite was over $125\mu\text{Wcm}^{-2}$. Meanwhile, in cyclic heating system, the peak power densities were generated with PMN-30PT single crystals at $8.64\mu\text{W/cm}^{3}$ at an angular velocity of 0.64rad/sec with a temperature gradient of 8.5°C/sec. The energy harvested by prestressed PZT composites was 40% larger than with simple PZT ceramics. Besides, simple analytic expressions are developed for ideal voltage, power and power densities as a function of pyroelectric constant, permittivity, surface area, thickness, temperature variation. The experimental trends show a pronounced increase (100% change in voltage) with surface area with the 0.1 GΩ resistance, but less pronounced for 10 GΩ (10% change in voltage).

CHAPTER 1 Introduction

With the instability of the energy prices and the advances in the electronics industry, energy harvesting has burgeoned in the last few years. Wireless sensors are an emerging technology that has the potential to revolutionize the monitoring of simple and complex physical systems. One of the biggest challenges with wireless sensors is power management. Two ways in which power can influence the hardware constraints of a wireless sensor are through the behavior of the power source and the power consumption of the system. Until recently the most popular energy source for a wireless sensor was a battery. Advances have been made in Very Large Scale Integration (VLSI) design which lowers power requirements of circuitry. This makes it possible for a sensor to have a long but finite life when used with a battery or a fuel cell. This also makes it possible for wireless sensors to harvest their own energy from the environment or from the system that it is monitoring. Thermal energy is a viable source for powering these devices. Traditionally this conversion has been done by generating a potential difference by using a temperature difference. Peltier devices have been the conversion device of choice. There is a demonstrated need to develop conversion devices that will outperform the Peltier device using other forms of technology. In recent years, piezoelectric materials have been exploited to convert thermal energy to electrical energy [Ujihara *et al*, 2007].This particular manner of energy harvesting will be described in detail in the next section.

1.1 Energy Harvesting

Due to recent advances in low-power portable electronics and the fact the batteries in general provide a finite amount of power, more attention has been given in the last decade to explore methods for energy harvesting and scavenging. As these devices are becoming smaller the power requirements are also getting smaller. Powering the densely populated nodes of a wireless networks is a serious problem due to the high cost of batteries. Batteries increase size, weight and energy harvesting provides a solution to this problem by scavenging energy from ambient sources such as wind, water, heat, light vibrations noise, etc and converting into useable form.

Energy harvesting is a process of converting energy that would otherwise be wasted, from surrounding environment or the parent system to power other wireless systems [Fay and Golomb, 2002]. One aim in energy harvesting is to effectively harvest energy from renewable energy sources. Another aim is to convert energy deemed useless into useful energy. Energy sources that are frequently squandered include solar, wind, water, indoor lighting, vibrations, acoustic noise, and temperature gradients. Others include the energy generated by humans from everyday activities such as walking, running or driving. Thermal energy which is often times ejected from a physical system as a loss can be converted back into useful energy which can be used to power an application such as a low power electronic device [Fay and Golomb, 2002]. Currently, a wide variety of thermoelectric materials are available and the appropriate choice for harvesting energy depends on their characteristics and properties. These materials utilize the Seebeck, Peltier, and Thomson effect to effectively convert heat into electricity. For example, a recent

2

commercial product, a wristwatch, uses environment modules to generate enough power to run the clock's mechanical components [Paradiso *et al*, 2005]. The thermoelectric modules work on the thermal gradient provided by body heat. Similar modules can be used for powering low power sensors used in structural health monitoring system. In this sense, they are attractive for recycling wasted heat into useable energy, and can be used to create highly reliable, silent and environmentally friendly energy harvesters [Rowe, 1995,1999; Wu, 1996]. One viable family of materials for this purpose is ferroelectric materials because of their inherent ability to convert heat into electrical energy. Harvesting these phenomena could be accomplished from the use of piezoelectric materials through the pyroelectric effect. Pyroelectricity is a property of a material whereby a voltage is produced as a result of a change in temperature. This allows the material to be used as a sensor (IR detectors) [Marult, 2001] and an actuator (Shape Memory Alloys as noise reduction devices) [Humbeeck, 2001].

1.2 Materials

Piezoelectric materials are materials that undergo transformations through physical interaction. Man-made piezoelectric materials are usually made from ceramics, that is an inorganic compound made up of a metal or semi-metal and one or more non-metals, therefore having a complex molecular structure. Some examples of ceramics include silica (SiO_2) and alumina (Al_2O_3). Ceramics that exist in an amorphous or non-crystalline phase may be classified as glassy while ceramics exhibiting a crystalline phase may be single crystal or polycrystalline. Crystals may be classified into seven systems based on geometry

that can be subdivided into thirty-two point groups based on symmetry of which twenty are piezoelectric. Out of twenty piezoelectric classes, ten can be termed ferroelectric, which is a material that contains a spontaneous dipole moment that can be reversed in an electric field. These ten crystal classes can also be termed pyroelectric. Some examples of these types of materials include $BaTiO_3$, $PbTiO_3$, $PbZrO_3$, $NaNbO_3$ and $KNbO_3$. Most commercially available piezo-ceramics have a perovskite structure where the basic chemical formula follows the pattern ABO_3, where A and B are cations of different sizes and O is oxygen. Lead Zirconate Titanate $Pb(ZrTi)O_3$ or PZT was discovered in the 1950s and is one of the most widely used piezoelectric materials. In the case of polymers, the piezoelectric effect was first observed in polyvinylidene fluorid polymer (PVDF) in 1969 and the pyroelectric effect was found several years later.

In spite of the large number of applications of piezoelectricity in existence, and the ones being developed, many studies looked into the possibility of harvesting energy through the use of these materials.   A brief history is summarized in the next section.

1.3 Piezoelectric Energy Harvesting

Extensive studies have been conducted into harvesting energy from vibrations using piezoelectric materials. Paradiso and Feldmeiser in 2001 using a piezoelectric element with a resonantly matched transformer and conditioning electronics that, when struck by a button, generated approximately 1mJ at 3V per 15N push, enough power to rum a digital encoder and a radio that can transmit over 50 feet [Paradiso and Feldmeier, 2001].   Antaki and his collaborators at the University of Pittsburg presented a shoe-

mounted piezoelectric generator in 1995 that they developed to power artificial organs[Antaki *et al*., 1995]. Their device incorporated two cylindrical tubes in the insole, each housing a PZT stack stimulated by a passive hydraulic pulser-amplifier. The amplifier converted low-frequency foot fall energy into an intense series of high frequency impulses that drove the PZT at its mechanical resonance. Although the prototype was slightly bulky and heavy, walking produced average power of 250-700mW, depending on the user's gait and weight, and a jog produced over 2W. Paradiso's team at MIT built a simpler integration of piezoelectric elements beneath a standard running sneaker's removable insole in 1998 and refined it in 1999 [Shenck and Paradiso, 2001]. The shoe scavenged energy from heel strikes by flattening an arrangement made from two back to back Thunder Unimorphs and from toe-off by bending a bimorph stave made from 16 layers of PVDF foil. Although the average power harvested was small, 8.3 mW at the heel and 1.3 mW at the toes during a standard walk, each shoe produced sufficient energy to transmit a 12-bit ID code via an onboard radio to the local area while walking [Kymissis *et al*., 1998].

The studies by Paradiso and Antaki were pioneering into demonstrating the feasibility of using piezos for energy harvesting. More recently Roundy et al. explored the possibility of scavenging vibrations as a power source for wireless sensor nodes [Roundy *et al*., 2004]. Using piezoelectric benders that exploit the 31 mode of operation, power densities of $375\mu W/cm^3$ were demonstrated, based on input vibrations of $2.25m/s^2$ at 120Hz. Simulations of optimal designs (altering the piezo geometry) demonstrate potential power densities approaching $700\mu W/cm^3$ from the same vibration source. Further work by

Roundy embedded a similar device inside automobile tires to produce power density of $1mW/cm^3$ at higher acceleration magnitudes of about $50m/s^2$ [Roundy, 2003]. Sodano, Inman and Park compared the energy generated by three different piezoelectric devices, PZT, Macro Fiber Composite (MFC), and the Quick Pack (QP). These devices convert mechanical strain into to electric energy by exciting them while attached to an aluminum beam. Each specimen was excited at resonance, subjected to a 0-500Hz chirp, and lastly exposed to random vibrations recorded from an air compressor of a passenger vehicle. This study concluded that the MFC performed poorly on power output because of it low capacitance. The MFC specifically is constructed using piezoelectric fibers and inter-digitized electrodes (IDE). This creates and array of capacitors that when connected in series the voltage adds but the current remains constant [Sodano, *et al*., 2003]. An important concept from this study is that impedance matching between the transducer and the circuit is critical when optimizing for power [Sodano, Lloyd, and Inman, 2004]. In generally, the study found the QP and the ceramic PZT material capable of recharging the selected batteries. However, in PZT was more effective in random vibration environments which are practically expected [Sodano *et al*., 2004].

The type of circuitry used to harvest the energy from a piezoelectric transducer is critical in achieving efficient transfer and is determined by the desired output to the load. The signal generated by the element is AC and needs to be rectified using an AC-DC converter into a useful one. The step down buck converter has been receiving wide spread recognition because of its efficiency. It consists of a diode in series with an inductor all in parallel with a capacitor with the switching of the rectified signal being accomplished by a

6

microcontroller or a MOSFET [Ottman *et al*., 2002]. Lefeuvre et al. has presented an approach to optimize the power flow of vibration based piezoelectric energy harvesting devices [Lefeuvre *et al*., 2005]. The optimization principle is based on the synchronization between extraction of the electric charge produced by the element and the system vibrations, which maximizes the mechanical to electrical conversion.   Theoretical predictions confirmed by experimental results show that the new principle increases the harvested power by 400% as compared with a quasilinear impedance adaptation optimization method.

Ottman, et al., modeled the power flow characteristics of a strain–type actuator that consists of two–piezoelectric layers encapsulated in a film, a Quickpack® model QP20W from Active Control eXperts (ACX).   Using this model they determined circuitry requirements needed to obtain optimal power flow in order to recharge a battery. A Quickpack excited by a shaker was used in the experimental setup along with an adaptive controller which sensed the battery current and adjusted the duty cycle accordingly. The results of this study showed that a DC-DC controller with adaptive control harvested energy at four times the rate of direct charging without a controller [Ottman *et al*., 2002]. Ottman, Hoffman, and Lesieutre expanded on this study by simplifying the control circuitry. They determined that a converter operating in discontinuous conduction mode would hold the optimal duty close to a constant as the excitation is increased on the transducer. This approach harvested energy at three times the rate of direct charging [Ottman *et al*., 2005].

All of the above studies have been performed on vibration energy harvesting using layers and stacks of piezoelectric materials such as PZT unimorphs, Bimorphs and PVDF films. Most of the energy harvesting studies deal with scavenging from vibrations, and a very few deal with harvesting from changes in temperature. The pyroelectric properties of the materials are largely ignored. The pyroelectric effect is a release of charge at the surface of the material when subjected to temperature changes. This property makes pyroelectric energy conversion suitable for applications both on earth and in space. Advances in materials and in thermal-electrical cycling methods are expected to provide low cost and high-power density electrical generators [Olsen *et al*., 1985b].

Early theoretical studies have shown that the conversion efficiency of pyroelectric devices was limited to <1% [Clingman and Moore, 1961]. Theoretical work by Drummond and Gonzalo indicated that much higher efficiencies (47% and 10-15%, respectively, for the two authors) might be possible [Drummon, 1975; Gonzalo, 1976] by using the copolymers of P(VDF-TrFE) that exhibit large piezoelectric and pyroelectric effect showed that the density of output electrical energy of conversion cycle is 30mJ/cm^3. Studies by Guyomar et al. have shown that a microgenerator composed of 8g of PVDF produces 0.32 mW power with 7°C temperature amplitude and 0.2Hz frequency [Olsen *et al*., 1985b; Guyomar *et al*., 2009; Sebald *et al*., 2006]. The same group has also theoretically predicted that PMN-PT single crystals could strongly improve the power generation.

In contrast to vibrations, temperature is mainly a slowly varying quantity due to the large heat capacity of the materials. Pyroelectricity is based on a pronounced temperature

dependence of the electric displacement field in a pyroelectric material. The pyroelectric energy harvesting which has received more and more attention is an attractive choice for improving power generation capabilities. These particular type of energy scavenging is described in the next section in detail.

1.4 Pyroelectric Energy Harvesting

Thermoelectric power generation has been confined to products based on Seebeck effect which was discovered in 1821. Whenever there is a temperature difference between the two points of the open circuit that is made up of two heterogeneous semiconductors, thermal electromotive force is produced, which is in direct proportion to the temperature difference between the two points. As mentioned in the RFP, commercially available thermoelectric generator modules (TGM) can provide of the order of 10 mW/cm^2 [Baert *et al*., 2006]. It is necessary to improve this power generation capability by an order of magnitude for wireless sensing applications. Thermal energy in the environment is a potential source of energy for low-power electronics. For example, a recent commercial product, a wristwatch, uses thermoelectric modules to generate enough power to run the clock's mechanical components [Paradiso *et al*., 2005]. The thermoelectric modules work on the thermal gradient provided by body heat. Similar modules can be used for powering low power sensors used in structural health monitoring systems. Ferromagnetic materials have been exploited to convert thermal into electrical energy [Ujihara et al., 2007]. In this sense, they are attractive for recycling wasted heat into useable energy, and can be used to create highly reliable, silent, and environmentally friendly energy harvestors [Rowe, 1995,

9

1999; Wu, 1996]. A recent patent was issued for energy harvesting using novel thermoelectric materials [Nesrsessioan *et al*., 2008], and batteries can be recharged using thermal gradients [Sodano *et al*., 2007]. One of the challenges of thermoelectric materials for energy harvesting is need for spatial temperature gradients.

The pyroelectric effect is another possibility for directly converting heat into electricity. Rather than harvesting energy from spatial temperature gradients, pyroelectric materials produce power from temporal temperature fluctuations [Whatmore, 1986]. In particular, charge is produced when the material's temperature is altered as a function of time; likewise, a change in temperature results in mechanical deformation. Recent work was presented on using PZT pyroelectric materials for energy harvesting and storage [Borisenok *et al*., 1996; Cuadras *et al*., 2006; Bauer, 2006]. Several factors must be considered to optimize the performance of such materials for a given application. For example, the material's geometry, boundary conditions, and even the circuitry used to harvest power must be carefully considered [Sebald *et al*., 2008]. The contributions of this work include investigating the potential application of thin pyroelectric materials for energy harvesting and examining the important parameters that affect power generation.

Pyroelectricity is based on a pronounced temperature dependence of the electric displacement field in a ferroelectric material. The pyroelectric effect, which has not been considered for thermal power generation so far perhaps because the electric current generated by pyroelectric effect is proportional to the time derivative of temperature, is an attractive choice for improving power generation capabilities. Further combining

10

piezoelectric and pyroelectric properties of material can result in a more efficient and realistic approach.

1.5 Summary and Objectives

The previous chapter provides a thorough background on energy harvesting technology. It further gives relevant information about the piezoelectric materials in energy harvesting, providing a detailed discussion on pyroelectric energy harvesting. A description of working principles involved in the energy harvesting are stated and reviewed.

Given the feasibility of harvesting pyroelectric energy from piezoelectric materials, the main objectives of this work are (1) To characterize electrical power scavenged from heat of available piezoelectric materials; and (2) To develop models to characterize electrical power based on material properties and environmental conditions. To this end this document is organized so that Chapter 2 gives brief definitions on the pyroelectric materials. The measurement of spontaneous polarization will be introduced in this chapter. The following chapter begins with a detailed description of experimental setup in the study. Using schematics, Chapter 3 also explains various experimental setups with static heating system and cyclic heating system used in the project.

The developments of models are provided in Chapter 4. This chapter has three subsections for the static heating system, cyclic heating system and the ideal power system. Results obtained through the experiments and the comparisons between the numerical and experimental results will be presented in Chapter 5. The summaries of discussions are also

provided in this Chapter. Finally, the last chapter states the conclusions drawn from the study and propose future directions that this research could follow.

CHAPTER 2 Background

2.1 Definitions of Pyroelectric Materials

A pyroelectric material is a material that exhibits, over some range of temperature, a spontaneous electric polarization that can be reversed or reoriented by application of an electric field. The pyroelectric effect is a property of the pyroelectric material which produces power from temporal temperature fluctuations [Whatmore, 1986].

Pyroelectricity is based on a pronounced temperature dependence of the electric displacement field in a piezoelectric material. The effect occurs in any piezoelectric material (single crystal, ceramic or polymer) which possesses a polar point symmetry. Microscopically, the pyroelectric effect occurs because of the asymmetric environment experienced by electrical charged species within the crystal structure of the material. This can be viewed schematically as shown in figure 1, which shows a two-dimensional lattice of cations and anions. The cations are displaced relative to the unit cells 'centre of gravity' to give rise to an electrical dipole moment (or spontaneous polarization P_s) along the line $(x_1 - x_2)$.
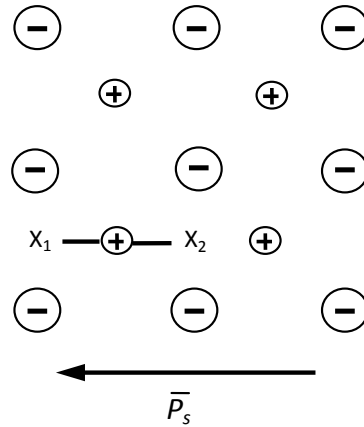
Figure 1 Schematic two-dimensional electrically polar lattice [Whatmore, 1986]

Quantitatively, the pyroelectric effect is described in terms of a vector, the pyroelectric

coefficient p, given by the rate of change of P_s with temperature (T) as shown in equation 1:

$$p = \frac{dP_s}{dT}$$ Equation 1

Polarization P is the electric dipole moment per unit volume. The polarization P

may be expressed as the bound surface charge per unit area of a free surface normal to the

direction of P. Polarization is related to electric displacement D through the linear

expression

$$D_i = P_i + \varepsilon_0 E_i$$

Equation 2

Where the derived constant ε_0 is equal to 8.854×10^{-12} C/V·m (permittivity of free space), E

represents the applied field, D is the electric displacement, P is the polarization as well. In

pyroelectric materials both D and P are nonlinear functions of E and may depend on the

previous history of the material. When the term $\varepsilon_0 E$ in the above equation is negligible

compared to P, D is nearly equal to P. Therefore, the D versus E and P versus E plots of

the hysteresis loop become, in practice, equivalent. In addition, permittivity is defined as

14

the incremental change in electric displacement per unit electric field when the magnitude of the measuring field is very small compared to the coercive electric field. The small signal relative permittivity, κ, is equal to the ratio of the absolute permittivity ε to the permittivity of free space ε_0, that is in Equation 3

$$\kappa = \varepsilon / \varepsilon_0$$

Equation 3

The value of the polarization Pr that remains after an applied electric field is removed is defined as the remanent polarization. The remanent polarization can be measured by Sawyer Tower Circuit which will be explain in the next section.

2.2 Measurement of Spontaneous Polarization (Sawyer Tower Circuit)

There are several ways are used to measure the magnitude of spontaneous polarization as well as the remnant polarization in pyroelectric materials. The Sawyer-Tower circuit is shown in Figure 2.
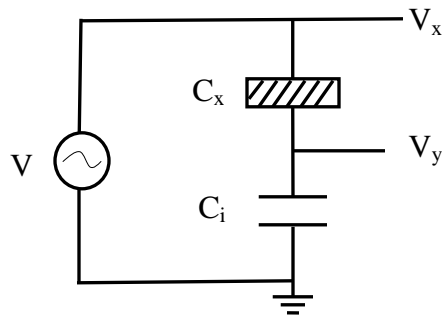
Figure 2 Sawyer - Tower circuit for observing hysteresis loops of pyroelectric materials
[IEEE standard definitions of primary ferroelectric terms]

The hysteresis loop of polarization versus electric field is recorded on an x-y plotter or an oscilloscope using Sawyer-Tower circuit. The interaction of hysteresis loop and y-axis is

15

remnant polarization. The value of P_s measured by this method usually depends on both the frequency and amplitude of the sine-wave voltage applied on the pyroelectric material. After applying high voltages, charge will be generated and measured through a capacitor and an electrometer. The charge and voltage are recorded using an oscilloscope and data acquisition system. Since P_s varies with the temperature, the pyroelectric discharge current on heating is given by Equation 4.

$$i = (\frac{dQ_s}{dT})(\frac{dT}{dt}) = \frac{AdP_s}{dT}(\frac{dT}{dt}) \qquad \text{Equation 4}$$

Where A is the area of the pyroelectric material, and Q_s is the total charge stored by the capacitor when the sample is heated from room temperature to a temperature above T_c.

For the piezoelectric materials, the charge generation is proportional to the temperature gradient as shown in Equation 2. The pyroelectric coefficient in the Equation 1 is the factor that describes the behavior of pyroelectric materials when subjected to the temporal temperature gradient. This coefficient is a function of spontaneous polarization P_s. Applying a large alternating electric field causes the polarization to reverse, and this gives rise to the pyroelectric hysteresis loop, relating the polarization P_s to the applied electric field E. A typical field-polarization loop is illustrated in figure 3.
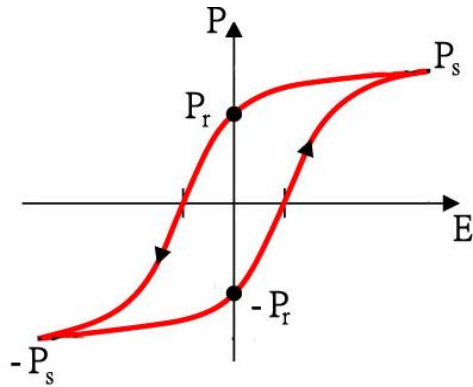
Figure 3 Hysteresis loop of a poled piezoelectric ceramic

The spontaneous polarization P_s is the polarization value when the electric fields E is at its maximum point.

The spontaneous polarization of piezoelectric materials is determined by the P-E loop at various temperatures. Generally, the existence of P-E Loop is considered as evidence towards establishing that a material is pyroelectric. Each piezoelectric materials has different pyroelectric coefficient.

CHAPTER 3 Experimental Setup

3.1 Heating System

In pyroelectric energy harvesting, temperature is one of slowly varying quantities due to the large heat capacity of the materials. As a consequence, a maximum of the available energy has to be harvested at one time. Heat sources may be static, i.e. temperature gradient available near power machines, or moving over time (exhaust gas, natural temperature variations due to convection, wearable element moving from inside to outside). It is always necessary to convert the temperature gradient into temperature temporal variation ($\Delta T/dt$) for this type of energy harvesting.

The power generation with a static and a continuous heating system are compared in this study. The experiments are conducted using a variety of commonly available pyroelectric materials: lead zirconate titanate (PZT single crystal $Pb(Mg_{1/3}Nb_{2/3})O_3-30PbTiO_3$ (PMN-30PT), and polyvinylidene difluoride (PVDF) .

To explore the effect of a non-cyclic and a cyclic temperature gradient, both systems are design and studied.

3.1.1 Static Heating System

In this case, the materials chosen for these experiments are PZT type OPT 5100 purchased from Omega Piezoceramics Inc., PMN-PT type TRS-X2A from TRS ceramics, and PVDF film by Measurement Specialties, Inc. with relevant properties listed in Table 1.

Table 1 Material Properties I

sample	Thickness (µm)	Area (cm^2)	Pyroelectric Coefficient (($µCm^{-2}K^{-1}$)	Capacitance (nF)	Curie Temperature (ºC)
PZT-5A	150	1.44	238	45 [i]	350 [iii]
PMN-PT	273	0.98	416	15 [i]	150 [iii]
PVDF	110	1.96	9	0.09 [ii]	165 [iv]

[i]measured, [ii]Malmonge *et al.*, 2003, [iii]APC Inc., [iv]Teyssedre, *et al.*, 1995

In order to achieve a constant heating rate, resistance heaters are chosen as the source of energy and connected with a feedback control system. The complete experimental system is shown in Figure 4, where the thin sample element was bonded to a thin resistance heater (Minco HK5578 R35.0L12B, 1.91cm × 1.91cm). The assembly was subjected to the ambient temperature and not in contact with any surfaces. The heater was used to control the temperature of the pyroelectric element and a Type K thermocouple sensor was attached to the backside of the resistance heater to measure the temperature of the heater. The measured temperature was assumed to be the temperature of the sample. The thermocouple sensor was passed through an Analog Devices AD595 monolithic thermocouple amplifier and the signal was recorded using a data acquisition system (National Instruments, LabPC+, 12-bit).

The block diagram of the system used to control the temperature of the heater is shown in Figure 5(a). The current amplifier circuit for the resistance heater is shown in Figure 5(b). The controller in the temperature control system is mainly used to control the heater in an effort to achieve the different heating rates as shown in Figure 6. Therefore,

the peak heating rates were set according to the operating temperature ranges of the

elements being tested.
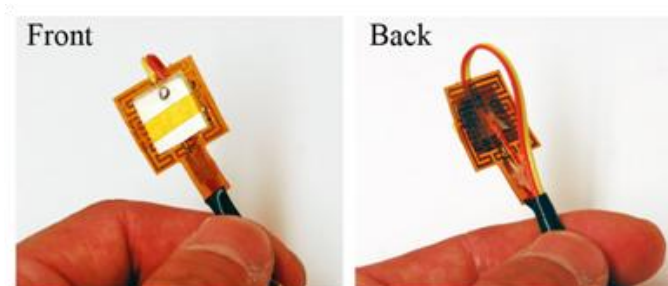
Figure 4 Photographs of front and back view of the PZT-5A sample mounted to a thin-film resistance heater.
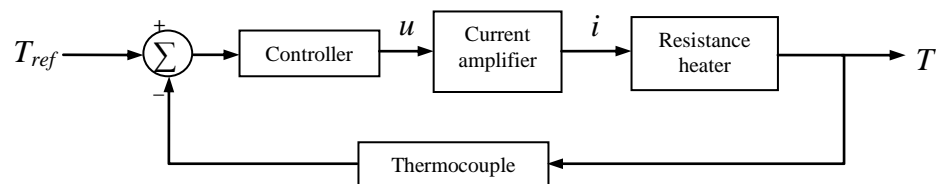
(a)
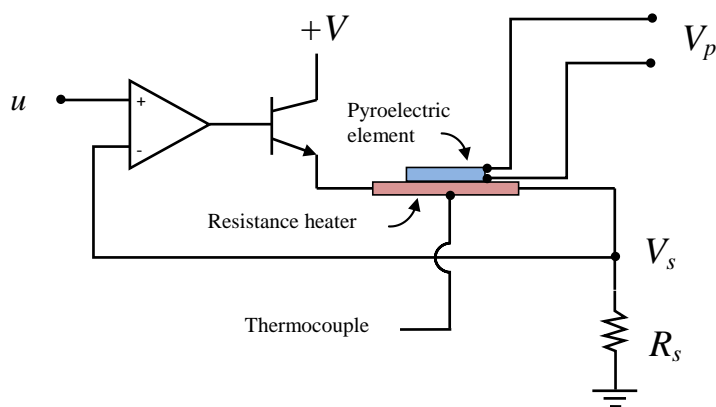
(b)

Figure 5 Experimental setup: (a) the block diagram of the temperature control system: (b) a schematic of the current amplifier, resistance heater, and thermocouple system.
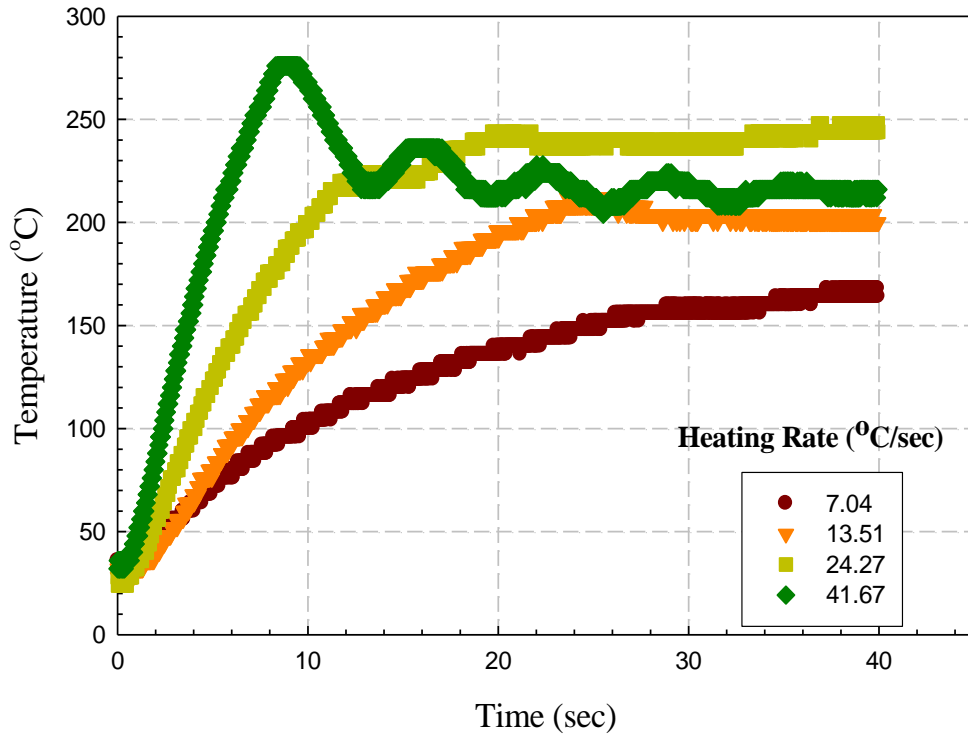
Figure 6 Different heating rates for static heating system

In addition to the different heating rates in a single impulse, a pulsating heating system is also explored. In the pulsating heating scheme the temperature spikes between high and cold regions. This periodic heating source may lead to continuous power generation over time. In this case, in addition to PZT, another material selected due to its high pyroelectric coefficient is selected, PMN-30%PT single crystals. The second pulsating heating scheme is described next.

3.1.2 Cyclic Heating System

In this case, a system is designed such that a periodic temperature is obtained. It consists of a rotating disk with an aperture controlled by a gear motor as shown in Figure 7. The rotating speed of the disc can be changed by controlling the voltage applied to the motor. The heat source is provided by a radiating heat lamp placed on one side of the rotating disk. The sensor is placed on a mounting plate on the opposite side of the disc facing the lamp. The heat is projected in the material sample through the aperture in the disc. As the disc rotates the sample is periodically heated. To maintain consistency, the sample is placed at a constant distance of 1cm from the disc during experimentation. A Type K thermocouple is used to monitor the temperature of the sample. It is assumed that the temperature of the mounting plate is equivalent to the temperature of the sample. The temperature is recorded electronically using a data acquisition system not shown in Figure 7. Typical heating profiles obtained with the system will be discussed and shown in Chapter 5 with different rotating speeds.

rotating disk

thermocouple sensor

gearmotor

test sample

holder

heat lamp
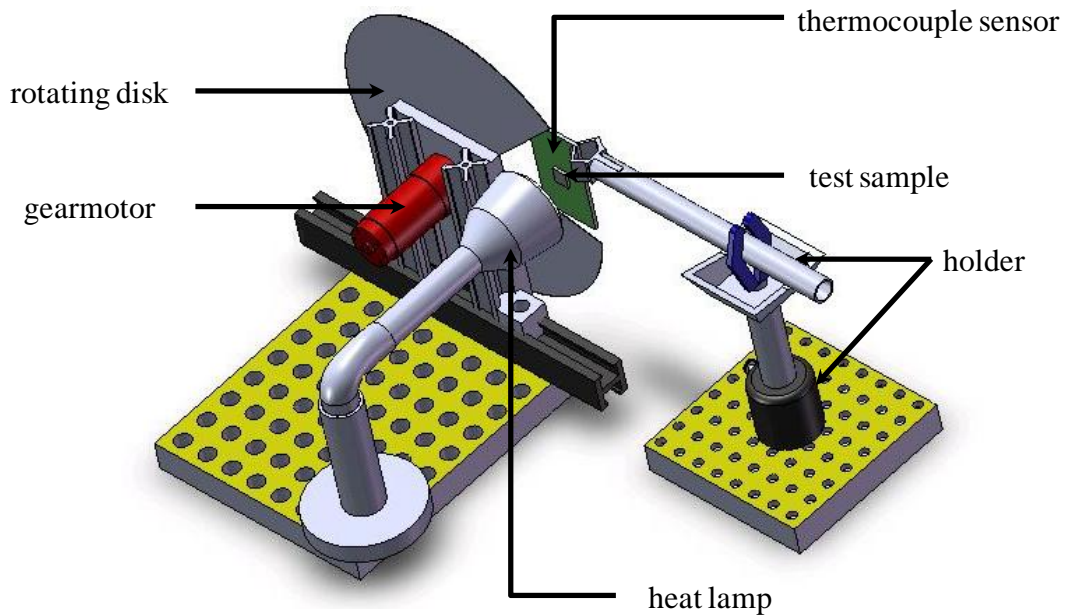
Figure 7 Cyclic heating system

The charge generated during the pyroelectric effect is a function of the materials properties and the surface area. Thus for higher power generation materials are selected with suitable properties maximizing volume. On these lines three pyroelectric samples are selected for the study, lead zirconate titanate (PZT), a prestressed PZT composite Unimorph and single crystal PMN-PT.

PZT is the most commonly used piezoelectric ceramic which has been studied extensively for its properties. It is also fairly inexpensive and easily available. The samples used on these experiments are plates purchased from Omega ceramics. Although PZT has fairly high electromechanical properties, it is brittle thus not very robust for implementing in certain application types. To overcome this limitation, several studies have been conducted into enhancing the properties of PZT ceramics by forming composites [Wise, 1998; Zhang *et al*, 2001]. The PZT composite selected for the current study is a Unimorph

with an adaptive PZT layer and two inactive metal layers forming a sandwich. The composite is made under high temperature and pressure such that the final product has an inherent curvature prestressing the ceramic. Due to this prestress the composite shows enhanced properties compared to the simple PZT ceramic [Mossi *et al*, 1998]. The composite is also very robust and can be easily made into several shapes and sizes.

Another material selected for the study was $Pb(Mg_{1/3}Nb_{2/3})O_3$-$30PbTiO_3$ single crystals (PMN-30PT). Single crystals of this type exhibit high pyroelectric coefficients and have been theoretically proven to generate large power densities [Olsen, et al 1985b; Clingman and Moore, 1961]. Thin plates with dimensions similar to the other selected materials were acquired for the study from TRS ceramics. Table 2 gives the dimensions and material properties for the selected devices. The energy is harvested using a static and continuous heating system and the power densities are measured using specially designed circuitry described in the following section.

Table 2 Material Properties II

Material	Area (cm^2)	Thickness (cm)	Capacitance (nF)
PMN-30PT	0.98	0.027	15
PZT-composite	1.44	0.02	9
PZT	1.59	0.025	45

3.2 Power Measurement System

3.2.1 AC-DC Converter Circuit

Electronic devices generally require direct current (DC) supply voltages. For this

reason, the alternative current voltage (AC) delivered by the pyroelectric element leads to be rectified. This is easily achieved by using an AC-DC converter circuit. This converter is usually composed of a rectifier bridge connected with a capacitor which acts as a filter removing ripples. Because of the high impedance nature of the pyroelectric materials, it is difficult to measure current using a traditional circuit as described in the literature review provided in Chapter 1. Thus in the current study, the circuit is modified to adapt to the selected pyroelectric materials by using an AD549 op–amp in the measurement system shown in Figure 5. The idea of this modification originated from the design of electrometers used to measure charge of small currents accurately. The AD549 was used to isolate the experimental setup from measurement system. The op-amp has an input bias current on the order of 150μA. Although it is extremely small, it is still three orders of magnitude larger than the current generation of the pyroelectric device which are expected to be in the order of nano amps. Hence input bias of the op-amp should have a negligible effect on the current measurements. The AD594 op–amp is a very delicate device and must be handled very carefully to avoid small bias currents caused by the electrostatic discharge shorting out the pyroelectric device. As shown in Figure 5, the pyroelectric element is represented by a current source in parallel with a capacitor[Park, 2001]. The resistance R is connected for impedance matching and the output voltage, V_o, is measured at the shown location. Each sample has a different capacitance thus for more efficient power conversion the value of R will be different for each element. Experiments are conducted to obtain an optimal value for R by testing several resistances in the range of $1 - 12M\Omega$ and the results are discussed in the chapter 5.

3.2.2 Power Measurement with Current Preamplifier

The electric circuit employed to measure the current across the PZT as shown in Figure 8. The PZT is represented as a current source in parallel with a capacitor. The pyroelectric current generated charges the capacitor. To measure the voltage thus generated without discharging the internal capacitor in the process of making the measurement is challenging. It is desirable then, to connect a large resistor in series that limits the current leakage. For example, for a 10V voltage developed and resistance of 10 GΩ, the current in 1 nA, which can be easily measured by a SRS 570 low noise current amplifier. The sensitivity of the amplifier is 1pA/V - 1µA/V and the gain accuracy of output is ±0.5%.

Pyroelectric element

R = 0.5, 5, 10GΩ

i_p

SRS 570
Lower Noise
Current Amplifier

A
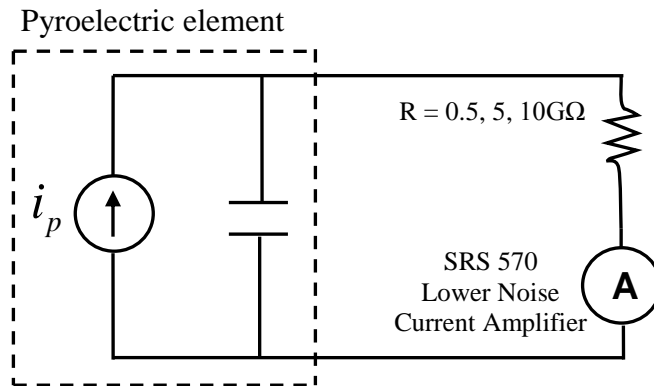
Figure 8 Experimental set-up to measure the voltage with current preamplifier across the pyroelectric sample.

CHAPTER 4 Modeling

In this chapter, a simple model is developed to predict the power generation based on the temporal change in temperature of the materials with two different heating sources. In addition, a simple analytical expression are developed for ideal voltage, power and power densities as a function of pyroelectric constant permittivity , surface area, thickness, temperature variation.

4.1 Static Heating System

A material as shown in Figure 9 is considered to exhibit the pyroelectric effect when a change in the material's temperature with respect to time (temporal fluctuation) results in the production of electric charge [Whatmore, 1986; Bauer, 2006]. In particular, the detectable current $i_p(t)$ of a pyroelectric material is proportional to the rate of change of its temperature [Whatmore, 1986].
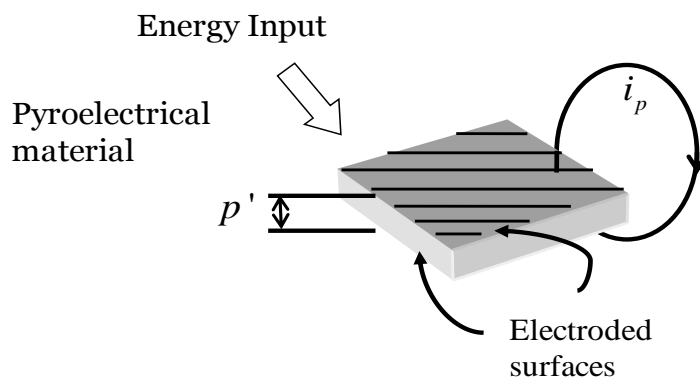
Figure 9 Electroded pyroelectric element showing flow of pyroelectric current due to change in temperature

$$i_p(t) = p'A\frac{dT(t)}{dt}$$

<div align="right">Equation 5</div>

where p' is the component of the pyroelectric coefficient vector p orthogonal to the electrode surface of area A; and $T(t)$ denotes the temperature with respect to time. For convenience, the heating and cooling behavior of the material is not considered.

A lumped–parameter model of a pyroelectric element is shown in Figure 10. The pyroelectric element is modeled as a current source $i_p(t)$ in parallel with an internal capacitance C_p. The figure also shows the pyroelectric element connected in parallel with an external capacitor C_e and resistor R_e. The objective is to determine the element's output voltage $V_p(t)$ and power $P(t)$ generated for a given temperature profile $T(t)$.

For a given temperature profile $T(t)$, the instantaneous power dissipated by the resistor R_e can be determined with knowledge of the output voltage $V_p(t)$,

$$P(t) = \frac{V_p^2}{R_e}$$

<div align="right">Equation 6</div>

On the other hand, the generated power can be predicted using Equation 1 as follows. Assuming zero initial conditions, summing currents in the circuit shown in Figure 1, the following relationship is obtained

$$p'AsT(s) = CsV_p(s) + \frac{1}{R_e}V_p(s)$$

<div align="right">Equation 7</div>

where s is the Laplace variable and $T(s)$ and $V_p(s)$ are the Laplace transforms of the input temperature and output voltage, respectively. The total capacitance C is the sum of internal capacitance, C_p and the external capacitance, C_e. Therefore, the transfer function relating the input temperature $T(s)$ to the output voltage $V_p(s)$ is expressed as

$$G(s) \triangleq \frac{V_p(s)}{T_s(s)} = \frac{p'As}{Cs + 1/R_e}$$

For a given temperature profile $T(t)$, the generated output voltage $V_p(t)$ across the pyroelectric element can be predicted by using Equation (8). Then, the power dissipated across the resistor can be calculated using Equation (6). The thermal dynamic effects such as the heating and cooling rate of the pyroelectric element are not captured in the above expression, Equation (8).

Appendix A shows the Matlab code used in the prediction of the power generation. The comparison between the measured and predicted results will be shown in chapter 5.

Pyroelectric element
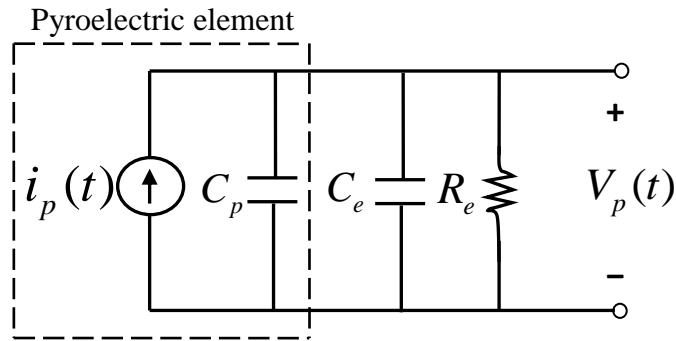
Figure 10 A lumped–parameter model of a pyroelectric element, which is modeled as a current source $i_p(t)$ in parallel with an internal capacitance C_p, connected in parallel to an external capacitor C_e and resistor R_e. The current $i_p(t)$ is proportional to the rate of change of temperature of the device. The voltage generated by the pyroelectric element is denoted by $V_p(t)$.

4.2 Modeling for Cyclic Heating System

Similar modeling techniques are considered in the cyclic heating system. However the biggest challenge were the quality of the experimental results with many unwanted signals associated with them. These signals have to be filtered in order to study details of

the energy conversion phenomena since usually energy is not measured directly. Using filters helps smooth a noisy signal and also reduces the error which arises during calculations of other quantities. Since the first differentiation of the temperature profile is necessary to accurately predict power, it becomes necessary to filter the signal. Direct differentiation of the experimental result amplifies the noise and generates erroneous results.

One of the obvious choices is a low pass filter. This choice is appropriate for this case since data is acquired at slow rates and it is corrupted by noise. Therefore, the principle of a low pass filter, which consists of replacing each data point by some kind of local average of surrounding data points, seems reasonable. Since nearby points measure nearly the same underlying value, averaging can reduce the level of noise without biasing the value obtained.

Specifically, the Savitzky-Golay filter is utilized for the modeling. Appendix B is the MatLab code for the prediction of the output power from a pyroelectric material is written using the Savitzky-Golay filter. The experimental data for temperature is filtered using the filter as well as the temporal temperature variation will be shown in the next chapter. The comparison of numerical and experimental results will be shown in chapter 5, as well.

The theory so far explored has aided on establishing formulae for energy conversion, however, the limits of pyroelectric energy conversion and power harvested is still unexplained. In the following sections, analytical expressions for the maximum voltage, current and power that can be harvested from pyroelectric materials are derived.

4.3 Analytical Model for Ideal Voltage and Power

An analytical expression for charge and voltage built up, instantaneous power and energy stored in the pyroelectric material is derived under open circuit condition, as shown in Figure 10. This is used to study the ideal maximum voltage, current and power density the material is capable of producing.

By definition the pyroelectric current produced is given by equation 5. It is independent of thickness. Thus the only geometric factor that directly influences it is the electrode surface area. Integrating equation 5 gives the charge that accumulates assuming no leakage as shown in equation 9.

$$q = CV = p'(\Delta T)A$$
<div align="right">Equation 9</div>

From equation 9 and capacitance of a flat plate given by equation 10,

$$C = \frac{\varepsilon_0 \varepsilon_r A}{h}$$
<div align="right">Equation 10</div>

The expression for voltage developed across the electrodes of the pyroelectric material is obtained (equation 11)

$$V = \frac{p'(\Delta T)}{\varepsilon_0 \varepsilon_r} h$$
<div align="right">Equation 11</div>

The voltage developed is independent of the electrode area of the sample and the only geometric factor that influences it is thickness. From equations 9 and 11 the instantaneous power developed is obtained (equation 12).

$$P = \frac{(p')(\Delta T)\dfrac{dT}{dt}}{\varepsilon_0 \varepsilon_r} Ah$$
<div align="right">Equation 12</div>

31

The power density (or power divided by volume) of the sample shown by equation 7 turns out to be independent of the surface area or height of the sample but solely dependent on the material constants, variation in temperature and temperature gradient.

$$P_{density} = \frac{(p')(\Delta T)\dfrac{dT}{dt}}{\varepsilon_0 \varepsilon_r}$$

Equation 13

Integrating equation 13 with respect to time and changing variables gives the expression for the total energy stored. This can be verified to be the same as the energy stored in a charged capacitor ($0.5CV^2$). The corresponding energy density can be obtained (equation 14.)

$$E_{density} = \frac{(p')^2 (\Delta T)^2}{2\varepsilon_0 \varepsilon_r}$$

Equation 14

Results are presented in the next section.

CHAPTER 5 Results and Discussion

5.1 Measured and Predicted Results for a Static Heating System

The control system described on section 3.1.1 was tuned to achieve a relatively high temperature rate which was slightly different for each element depending on their properties and the ambient temperature. The average heating rate for all samples was 16.6°Cs^{-1}. The results of each case are discussed in detail below.

In case of the PZT, a temperature range of 29.79 to 102.78°C was used for the experiments, achieving a peak heating rate of 15.65°Cs^{-1} [see Figure 11(a)]. The resulting measured and predicted output voltage profiles V_p for the PZT-5A element are shown in Figure 11(b). As seen in the graph, both the profiles are in good agreement. Similarly, the profiles for power are also compared as shown in Figure 11(c). Like the voltage results, the measured and predicted calculated dissipated powers are in good agreement, taking on values of 0.28μW and 0.33μW, respectively. The power densities were determined by normalizing the power measurements with the sample area given in Table 1. The peak power densities for the numerical and experimental results were 0.23μWcm^{-2} and 0.20μWcm^{-2}, respectively.
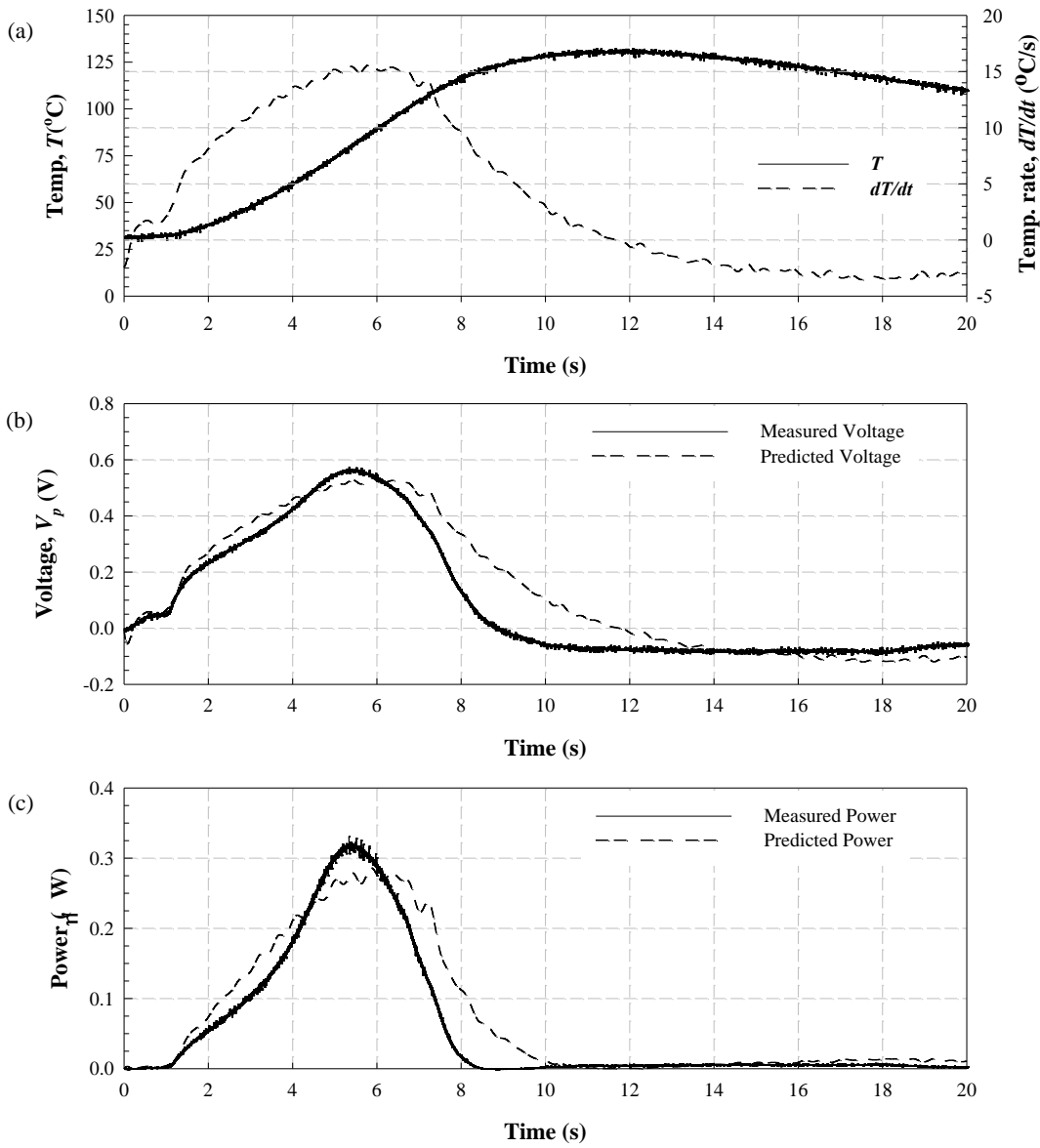
Figure 11 Measured and predicted results of power generated by PZT-5A element. (a) Temperature and temperature rate (dT/dt) vs. time; (b) Measured and predicted PZT voltage vs. time; and (c) Measured and predicted power vs. time

Similarly, experiments and simulations were conducted with a PMN-PT sample where the results are shown in Figure 12(a) – (c). The temperature range was from 22 to 103.9ºC, achieving a heating rate of 14.45ºCs^{-1} as shown in Figure 12(a). The measured

and predicted peak voltages were 0.57V and 0.59V, respectively, as shown in Figure 12(b). Not only does the experimentally obtained power follow the predicted profile closely [Figure 12(c)], but also, the peak power values were in good agreement at 0.33μW and 0.35μW. As in the case of PZT, power densities were determined for PMN-PT with the measured and predicted results of 0.33μWcm^{-2} and 0.36μWcm^{-2}, respectively. In all cases the differences between the predicted and measured results were less than 10%.

Results for the third material tested, PVDF, are shown in Figures 13(a) − (c). Temperatures in this case ranged between 30 to 141ºC with a resultant heating rate of 19.64ºCs^{-1} as shown in Figure 13(a). Peak voltages of 0.49 and 0.51V were obtained experimentally and numerically [see Figure 13(b)]. The power profile are shown in Figure 13(c) resulting in maximum power of 0.24μW and 0.26μW and power densities of 0.12μWcm^{-2} and 0.13μWcm^{-2} for calculated and predicted values, respectively.

All the results are summarized in Table 2. As evident in the table the best match, with the smallest difference between measured and predicted results, is seen in the case of the PMN-PT samples, followed by PVDF and PZT samples. Differences in the voltage readings of only 4% are seen for the PMN-PT samples. Also the largest power generated is with PMN-PT even though it has a comparatively smaller area. This can be explained by its significantly larger pyroelectric coefficient. With dimensions similar to the PMN-PT sample used in the experiments, the power density for a lead scandium tantalite (PST) sample with pyroelectric coefficient $p' = 6000\mu$Cm^{-2}K^{-1} is determined to be 125μWcm^{-2}, which is approximately three orders of magnitude larger. Another enhancing factor could be its large thickness, although it is not included in the model calculations. Thickness

could indirectly affect the temperature gradient required to generate a current, thus affecting the power generation. Since the PMN-PT sample was comparatively much thicker than the rest of the materials (82% more than PZT), a peak temperature of 103℃ could be used safely in spite of having a low transition temperature of 80℃ without damaging the sample. Following PMN-PT, the next largest power density was with PZT, then with PVDF. This trend was expected because of the ordering of the pyroelectric coefficient. While comparing with another energy harvesting source such as vibrations, the energy densities generated by PZT energy harvesting are much higher, 32mWcm^{-2} [Lu *et al*, 2004] and 400μWcm^{-2} [Roundy and Wright, 2004]. But since thermal gradients are readily available in many places, a combination of vibrations and heat could prove as a potential source of efficient energy harvesting.

Figure 12 Measured and predicted results of power generated by PMN-PT element. (a) Temperature and temperature rate (dT/dt) vs. time; (b) Measured and predicted PMN-PT voltage vs. time; and (c) Measured and predicted power vs. time.
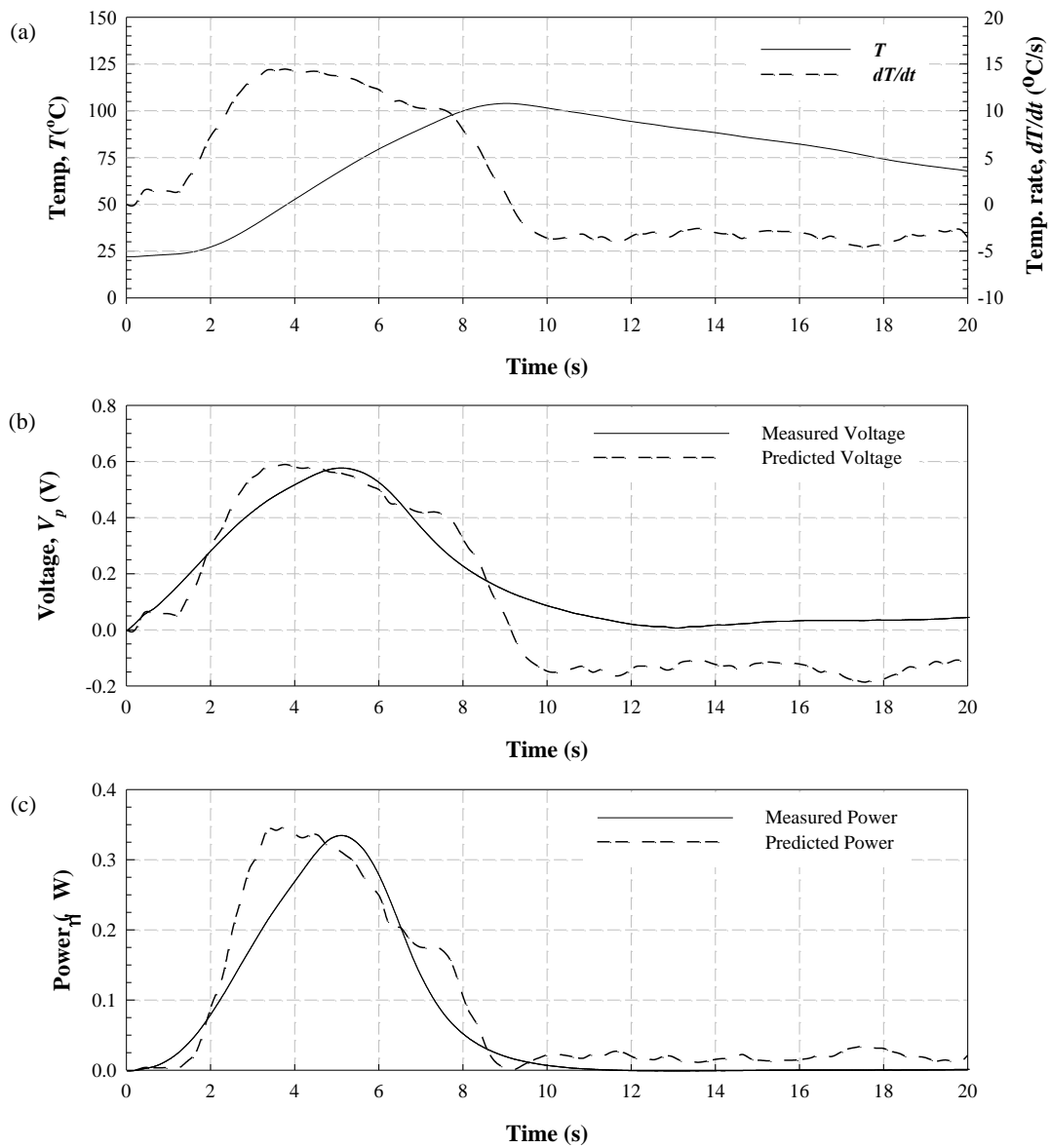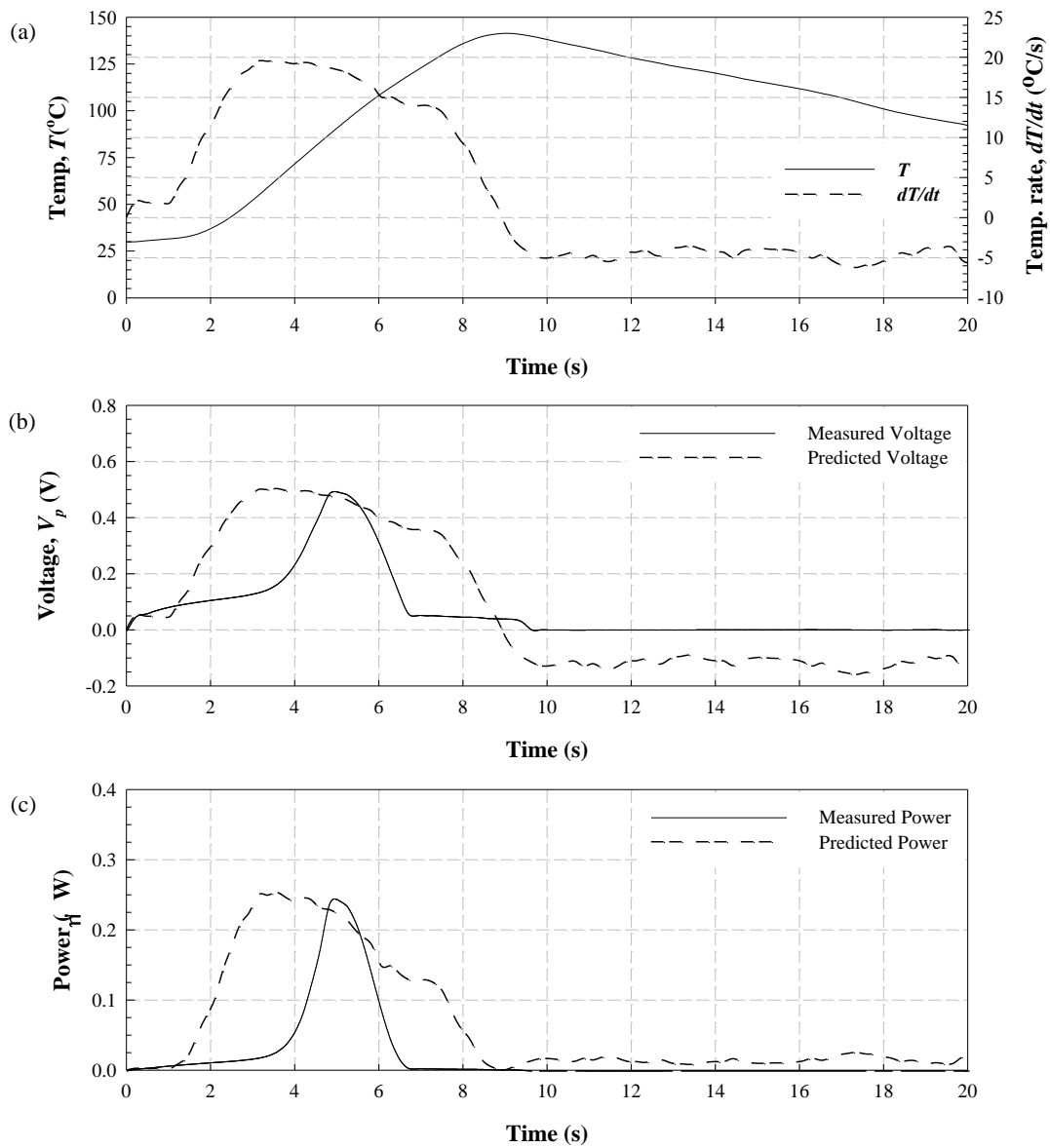
Figure 13 Measured and predicted results of power generated by PVDF element. (a) Temperature and temperature rate (dT/dt) vs. time; (b) Measured and predicted PVDF voltage vs. time; and (c) Measured and predicted power vs. time.

Table 3 Measured and predicted result comparison for static heating system

Sample	Peak Voltage (V)			Peak Power(μW)			Power Density(μWcm^{-2})		
	Measured	Predicted	Difference	Measured	Predicted	Difference	Measured	Predicted	Difference
PZT-5A	0.53	0.58	9%	0.28	0.33	16%	0.20	0.23	14%
PMN-PT	0.57	0.59	4%	0.33	0.35	6%	0.33	0.36	9%
PVDF	0.49	0.53	8%	0.24	0.26	8%	0.12	0.13	8%

It is important to note that there could be discrepancies in the results attributed to several factors. First, the temperature of the element was measured at a single point using the thermocouple sensor, and thus temperature may not have been uniform across the sample. Second, the temperature was measured on the backside of the resistance heater and was assumed to be the temperature of the sample. This assumption was made because of the relatively thin samples were used and the transient spatial temperature behavior across the thickness of the sample was ignored. In case of PVDF, the material exhibited above average bonding characteristics at the interface between the heater and sample, and this could have introduced some error in the measurements.

To study the potential of using other pyroelectric materials for power generation, the model given by Equation 8 combined with the measured temperature profiles shown in Figure 11(a), Figure 12(a), and Figure 13(a) were used to predict power generation of samples with different sizes other than the ones tested experimentally. The model was also used to make predictions for materials with higher pyroelectric coefficient than the ones tested to further illustrate the potential that larger pyroelectric coefficients enhance the power generation. In particular, thin-film lead scandium tantalite (PST) with pyroelectric coefficient $p' = 6000\mu Cm^{-2}K^{-1}$ [Watton and Todd, 1991; Todd *et al.*, 1999] and lead

magnesium niobate - lead titanate (PMN-PT) with $p' = 300$ to over $1000\mu Cm^{-2}K^{-1}$ [Sebald *et al.*, 2008; Kumar *et al.*, 2004] were considered.

Figure 14 shows the peak power density as a function of area and pyroelectric coefficient. The area was varied between $1.44cm^2$ ($1.20cm \times 1.20cm$) to $3.63cm^2$ ($1.91cm \times 1.91cm$) and the capacitance was adjusted accordingly by assuming a constant electrode separation for a parallel–plate capacitor model. The pyroelectric coefficient was varied between $p' = 238\mu Cm^{-2}K^{-1}$ and $p' = 6000\mu Cm^{-2}K^{-1}$. The maximum power density calculated with these values was $340.875\mu Wcm^{-2}$. The predicted result shows the potential for using thin-films with improved pyroelectric coefficient, as well as maximizing the area of the energy harvesting element. These results point out the importance of maximizing these terms for energy harvesting.
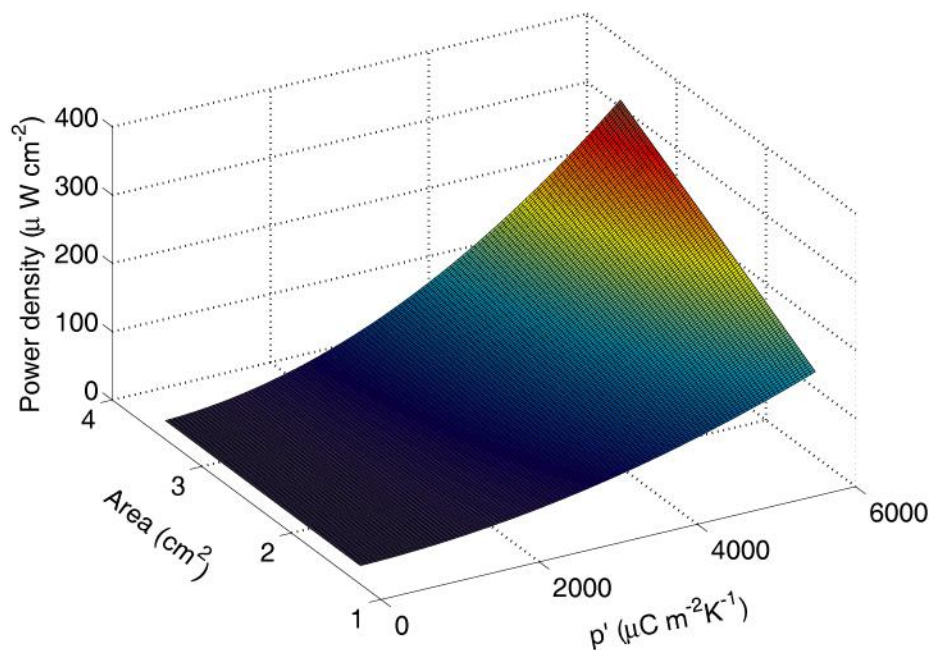
Figure 14 Predicted peak power density as a function of pyroelectric coefficient and area based on same boundary conditions as the experiment on PZT-5A

5.2 Results and Discussion for Cyclic Heating System

In this case, typical heating profiles obtained with the cyclic temperature gradient system are shown in Figure 15 with three rotation speeds of 0.64, 1.53, 3.34 rad/sec. At smaller rotating speeds the temperature gradient, ΔT, is larger as the samples are exposed to the heat lamp for longer periods of time allowing the sample to get hotter. Several rotating speeds, ω, are tested to observe its effects on power conversion.
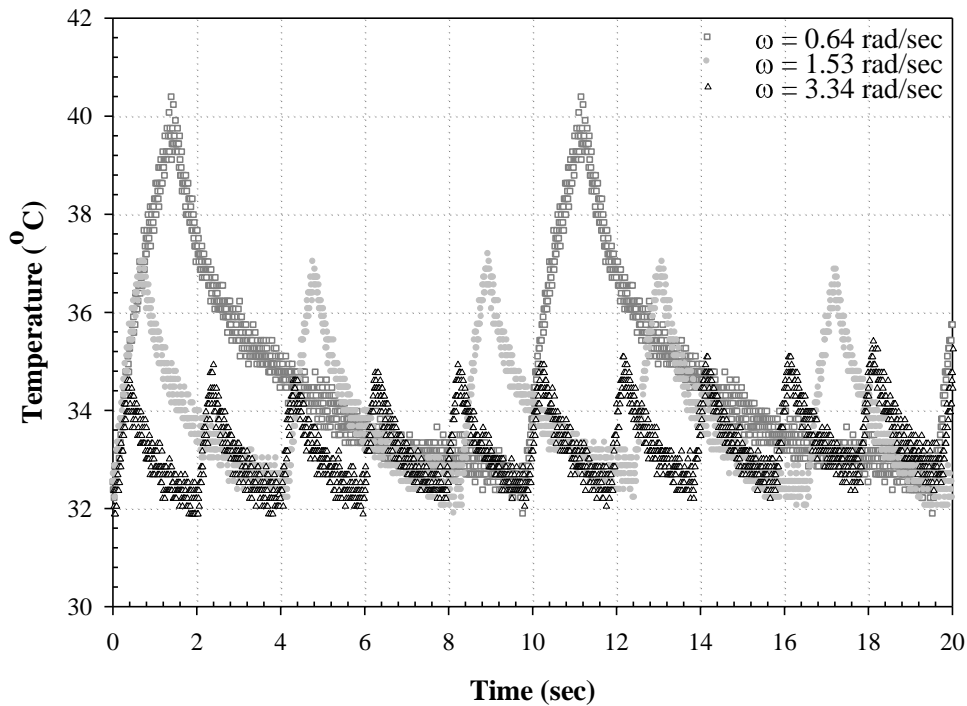
Figure 15 Cyclic heating profiles at different angular velocities

With the static (system described in 3.1.1) and continuous heating systems (system described in 3.1.2) the voltage generated V_o is measured. A typical voltage profile obtained with a PZT element for the static heating system using a circuit resistance of 7MΩ is shown in Figure 16. As seen in the graph (Figure 16) voltage is generated when

41

temperature increases, and when a stable temperature is maintained the generation drops to zero. Thus a temperature gradient causes a generation of power as indicated by others [Whatmore, 1986]. From the measurements, power is calculated with the standard power relationships of voltage and current. With a heating rate of 15ºC/sec a peak power density of approximately $15\mu W/cm^3$ is measured. Due to the direct relationship with temperature gradients it is expected that larger gradients will yield more power, however this phenomenon of large gradient is rare and not very practical [Whatmore, 1986].
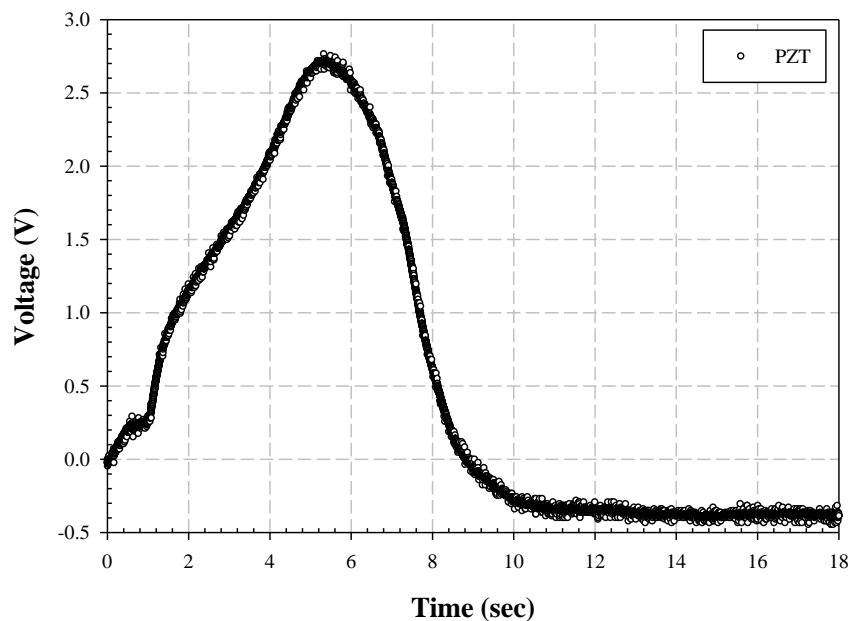
Figure 16 Measure PZT voltage with static heating at a temperature

Thus to generate more power over time a cyclic heating system is more applicable. Figure 17 shows a typical power density profile obtained with the cyclic heating system proposed. The temperature gradient obtained in this case is much smaller at 8ºC/sec, thus the power generated is also smaller. The gradient can be increased by varying the period of the heating system. The period is controlled by the rotation speed of the disc. The peak

power density obtained for PZT using a sample circuit resistance of 7MΩ is 8.64μW/cm³.
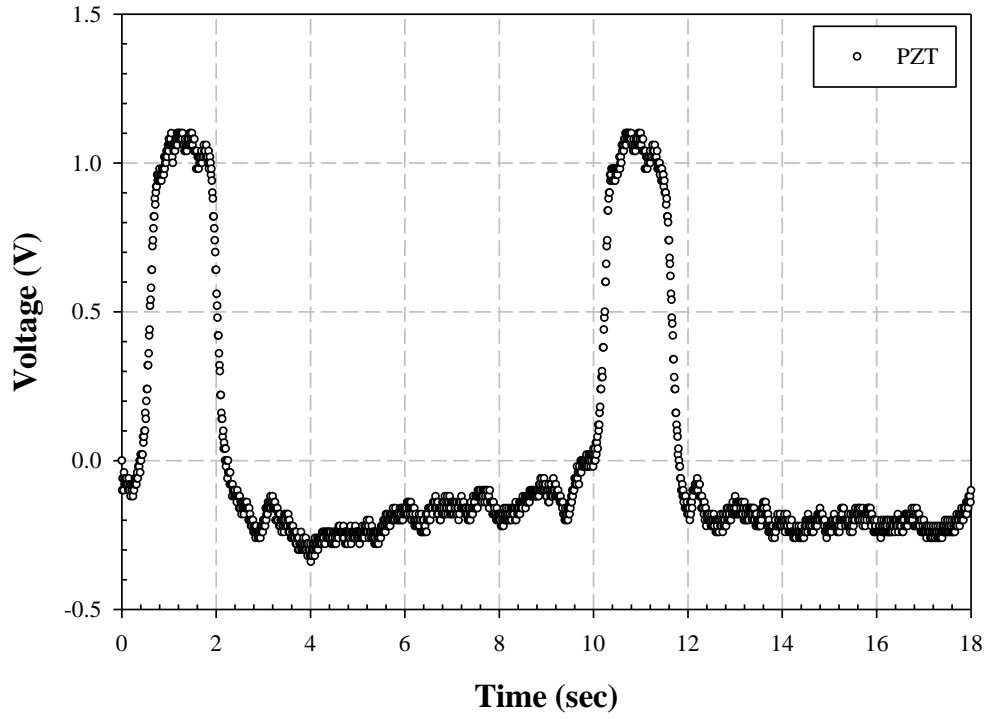
Figure 17 Measure PZT voltage with static heating at a temperature gradient of 8.5ºC/sec

To test the period effect, the disc is operated at several speeds ranging from 0.5 – 12.5 rad/sec. Each speed has a different temperature gradient as shown in Figure 15. The experiments are conducted at a constant R of 7MΩ for all samples to maintain consistency for a valid comparison. Later on in the study R is optimized for each element. The effect of ω can be observed from Figure 18. As seen in the graph as ω increases the power density decreases. At faster speeds, ω, the temperature gradient, ΔT, is very small, thus the power generation is also small. This is in agreement with the function of the pyroelectric effect described in Equation 2. The charge detected as a current i_p, flows in an external circuit depicted by Equation 2 [Whatmore, 1986]. In the equation dT/dt is the temperature

43

gradient, p' is the perpendicular component of the pyroelectric coefficient and A is the surface area of the element. As dT/dt is directly proportional to i_p, the power generation will be greater at higher gradients. Although the power densities generated by the cyclic heating system are smaller over time the total energy generated is larger when accumulated over time.

$$i_p = Ap' \frac{dT}{dt}$$

Equation 2
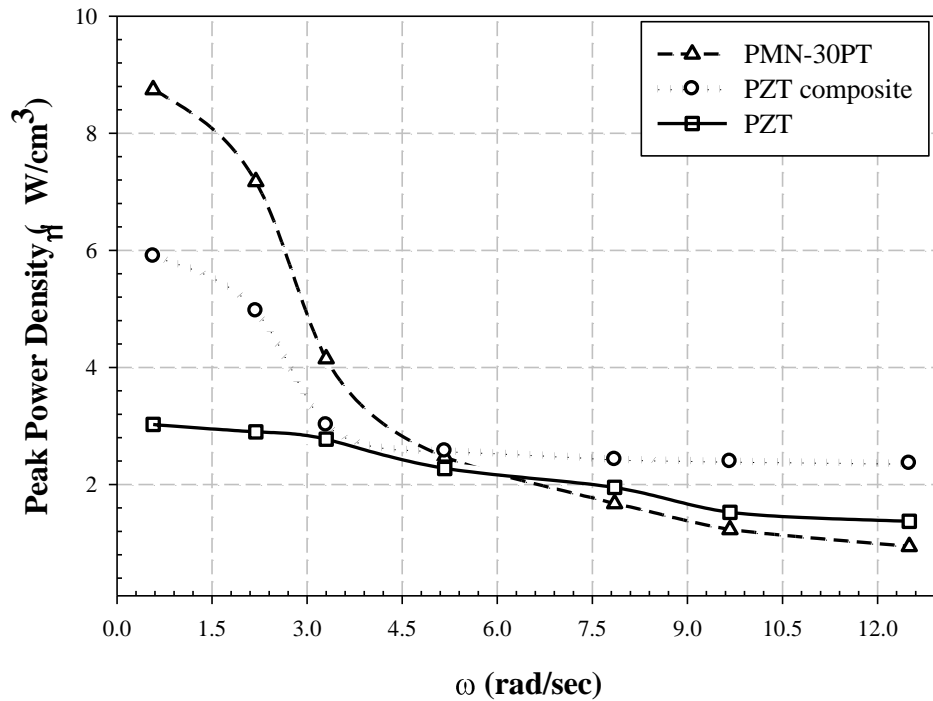
Figure 18 Effect of ω on power density with cyclic heating

To optimize power management the resistance R used in the circuit was tested for a range of values from $1 - 12M\Omega$ at all the tested speeds. A typical result at ω of 1.64 rad/sec is shown in Figure 19 for all materials tested. Although the figure shows results for a selected few, all tested speeds presented similar patterns. Based on these tests, the optimal value was determined as $8M\Omega$ for the PZT samples. For the other two materials,

the PZT composite and PMN-PT, the power density did not peak in the tested range of

resistances. The power generated with PMN–PT appears to be peaking toward the end of

the range but further experimentation is required to determine an exact value. This could

be due to the higher impedance of PMN-PT and PZT composite compared to PZT arising

from the lower capacitance. This also demonstrates that the composite has different

properties than the ceramic and the prestress plays some role in its behavior. The enhanced

performance of the PZT composite can also be observed in the magnitude of the peak

power densities. As shown in Figure 19 the power densities generated by the PZT

composite are approximately 40% higher than PZT ceramic.
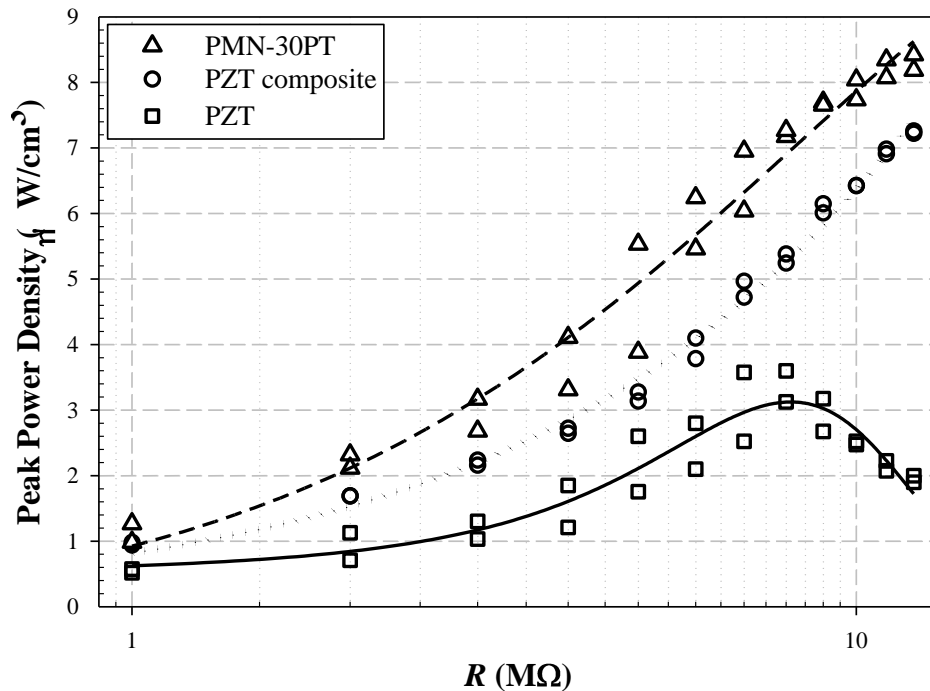
Figure 19 Optimal resistance *R* for power measurement circuit

Figure 20 shows typical power density curves at ω of 0.64rad/sec with the three

tested elements. The largest power generated is with PMN-30PT in agreement with the theoretical studies listed in the literature [Guyomar, *et al*., 2009; Sebald *et al*., 2006]. The peak power density measured with PMN-30PT is 8.64µW/cm^3, followed by PZT composite of 6.31µW/cm^3 and PZT 4.48µW/cm^3.
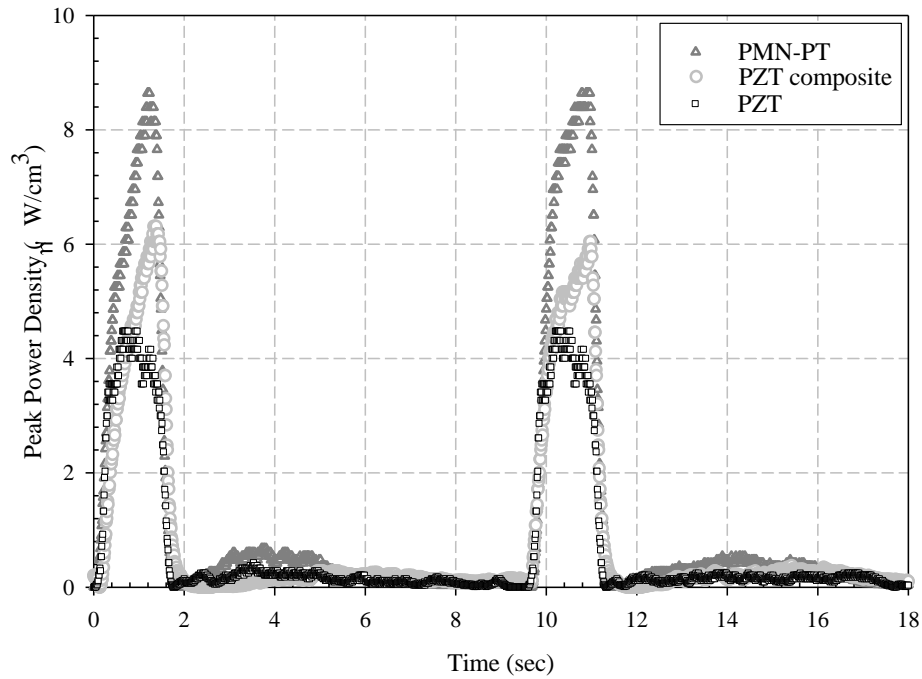
Figure 20 Power density comparison with ω of 0.64rad/sec

To further explain these results the pyroelectric coefficients of PZT and prestressed PZT composite are measured using the Sawyer and Tower circuit method described in the IEEE standards STD 180-1986. The pyroelectric coefficient of the PZT composite is more than two times higher than PZT as shown in Figure 21. This explains the larger power generation with the composite elements in agreement with the direct relationship of coefficient and power as indicated by Equation 2. Table 3 lists the peak measured power densities and equivalent pyroelectric coefficients for each element.

46
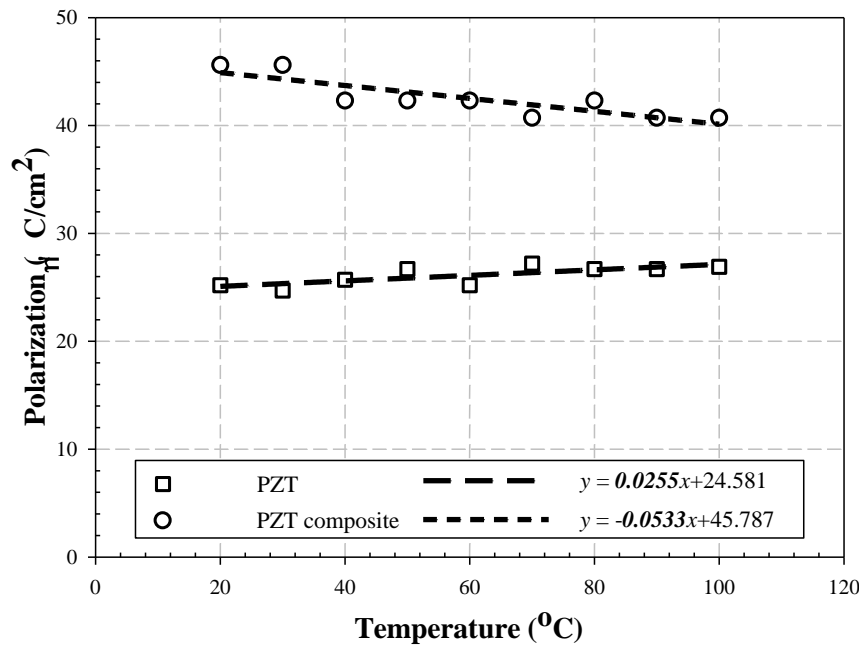
Figure 21 Measured pyroelectric coefficients of PZT and PZT composite using the Sawyer and Tower circuit

Table 4 Summary of results for the cyclic heating system

Pyroelectric Coefficient Material	Peak Power Density ($\mu W/cm^3$)	Pyroelectric Coefficient ($\mu C/cm^{-2}K^{-1}$)
PMN-30PT	8.64	0.086
PZT-composite	6.31	0.053
PZT	4.48	0.026

The results demonstrate that a cyclic heating source provides a means of continuously harvesting energy. The energy harvested in this manner is smaller than the energy harvested using a static heating source. In traditional methods all the energy has to be harvested at once which leads to lower efficiency. With cyclic heating the temperature gradients are smaller but over time the total energy harvested can accumulate to be larger.

The temperature profile and the temporal temperature variation are shown in the figure 22. The temperature profile obtained with respect to time for the pyroelectric material when heated periodically is shown in figure 22(a). The graph is not smooth because of the fact that the temperature data is affected by the noise. The same temperature profile for the pyroelectric material after the application of filter is shown in figure 22(b). Using filter has helped to smooth the noisy signal. The temporal temperature variation of the noisy temperature profile is as shown in figure 22(c). The graph shows the effect of noise on the experimental data. The noise signal gets amplified on differentiation and thus generates erroneous result, as it can be seen from the graph. The temporal temperature variation for the filtered temperature profile is as shown in figure 22(d). This graph makes some sense as when a material is heated the rate of temperature rise is more at the start and then it gradually decreases and finally becomes zero. Since the material is allowed to cool therefore the rate of temperature is negative for a finite time. The graph is periodic as the material is exposed to a periodic heat field.
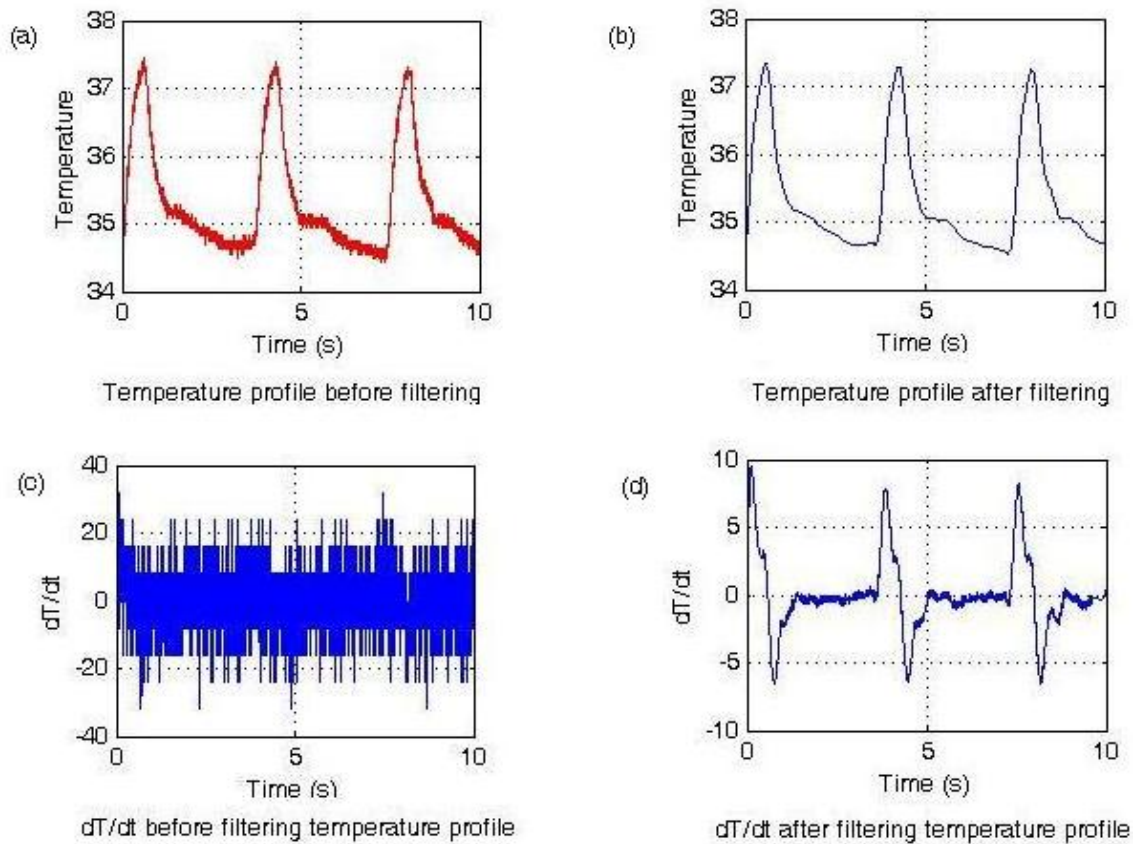
Figure 22 The experimental and filtered temperature profile: (a) the experimental temperature profile: (b) the filtered temperature profile: (c) the temperature rate using experimental data of temperature: (d) the temperature rate using filtered temperature profile

The dT/dt value obtained before filtering temperature profile shows how the direct differentiation of experimental results amplifies the noise signal. The dT/dt value obtained after filtering the temperature profile is in good agreement with the predicted values using the data of voltage profile.

The current and hence output power is predicted for all the three materials: PZT, PMN-PT, and Square Thunder. The value of the materials' properties used for the

49

calculations are shown in table 5. The power for different materials was measured across an external resistor having resistance value 7MΩ.

Table 5 Material properties III

Material	Pyroelectric coefficient ($\mu Cm^{-2}K^{-1}$)	Capacitance (nF)	Area (mm^2)
PZT	238	45	158.76
PMN-PT	416	17.4	98
Square Thunder	500	9.3	144

The measured and predicted calculated power profiles for all the three materials are shown in figure 23. The predicted power for the PZT was in good agreement with the experimental result, but for PMN-PT and Square Thunder it shows very large deviation from the experimental results (reasons yet to find and discuss).In case of PZT, the power profile is nearly the same as obtained using experimental values.

Energy obtained from any system can be calculated using the power profile and is equal to the area under the graph. The measured and calculated predicted energy obtained from all the three materials were calculated. In order to verify the accuracy of the mathematical model the difference between the measured and the predicted energy is calculated and hence the error.

$$\text{Error} = \frac{\text{Calculated Predicted Energy} - \text{Calculated Measured Energy}}{\text{Calculated Measured Energy}}$$

The results are shown in table 6.

Table 6 Comparison of measured and predicted results for cyclic heating system

Material	Measured Energy (μJ)	Predicted Energy(μJ)	Error (%)
PZT	0.2410	0.2560	6.23
PMN-PT	0.3265	0.6130	87.73
Square Thunder	0.3034	2.3250	666.36

The predicted power calculated was mapped with the power obtained experimentally. In case of PZT, the measured and predicted result is in good agreement, and the measured and predicted energy value shows an error of 6.23%, which is acceptable. In case of PMN-PT, the measured and predicted result is not in good agreement with each other, and the measured and predicted energy value shows an error of 87.73%. Similarly, the error in case of Square Thunder is also very high and is 666.36%.

.
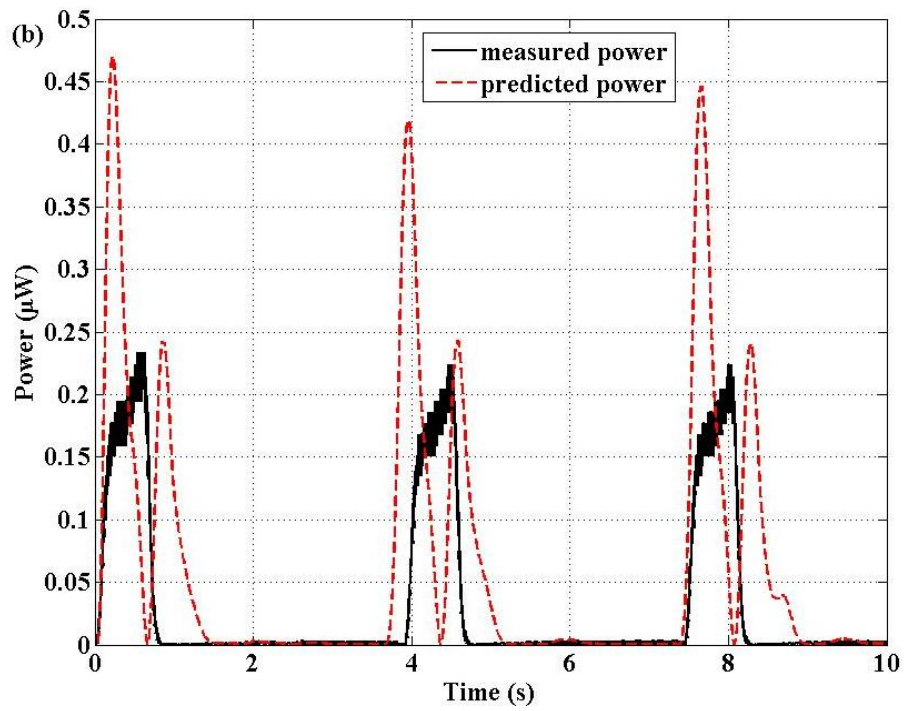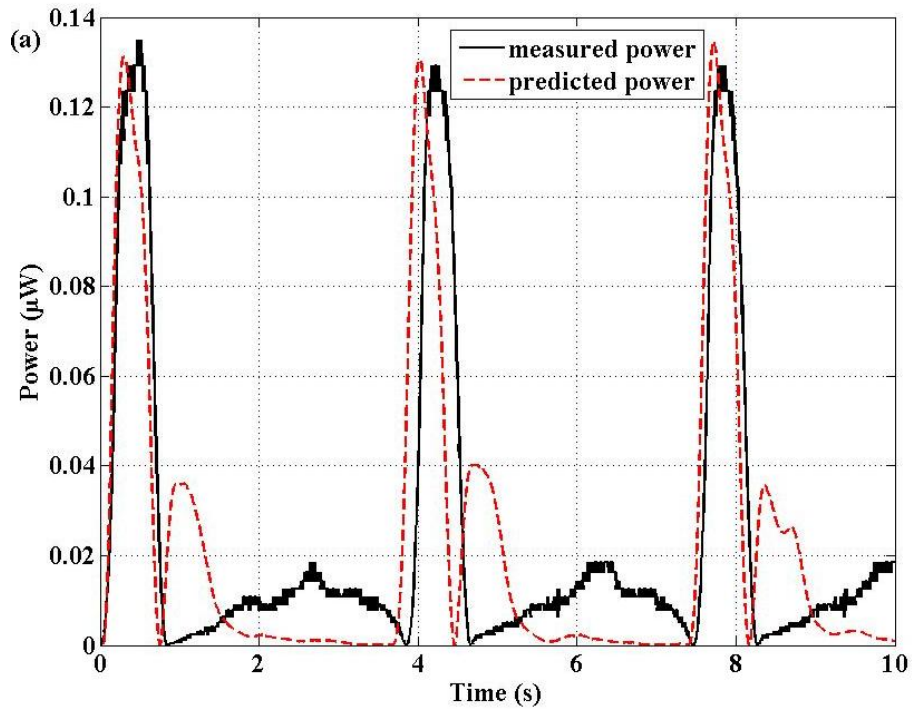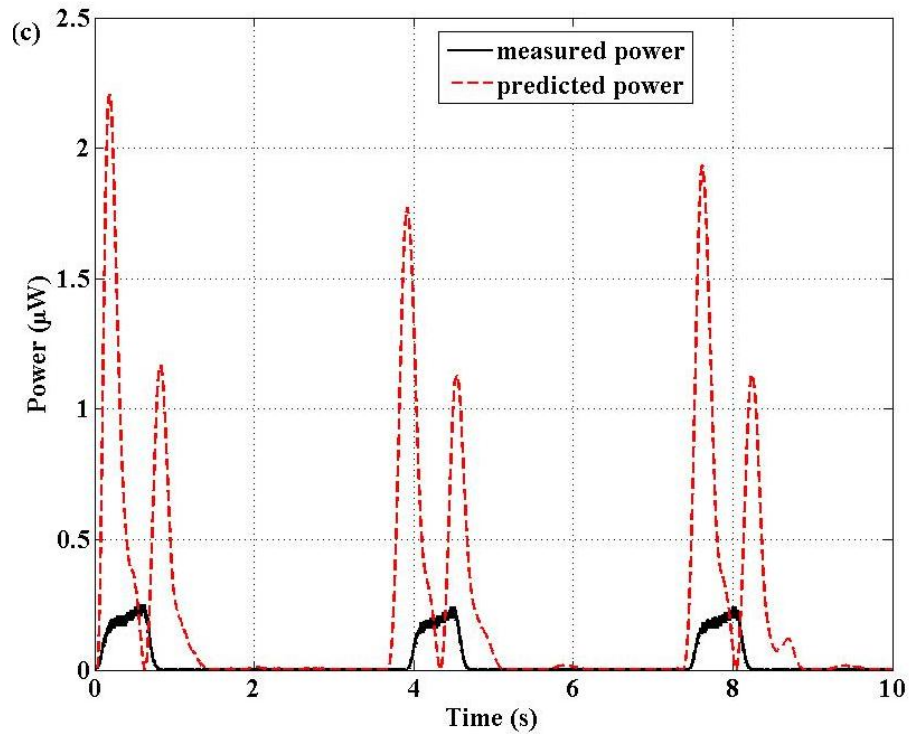
Figure 23 Measured and predicted results of power generated during cyclic heating. (a) For PZT; (b) For PMN-PT; (c) For Square Thunder

5.3 Results for the Ideal Model

One set of experiments involve obtaining polarization vs. electric field behavior at different temperatures (Figure 24). These are necessary to characterize the remnant polarization (P_r) and slope near P_r as a function of temperature (Figure 24), which in turn determines the pyroelectric coefficient and relative permittivity as a function of temperature. These constants along with the physical dimensions of the samples determine the theoretical voltage, current and energy that can be harvested from the pyroelectric material.

Another set of experiments (Figure 25) determine the voltage harvested due to variation in temperature. Obtaining this for various thickness and surface areas will determine the extent to which scaling relations developed in this paper are valid.

Experiment for polarization vs. field curves, permittivity and pyroelectric coefficient
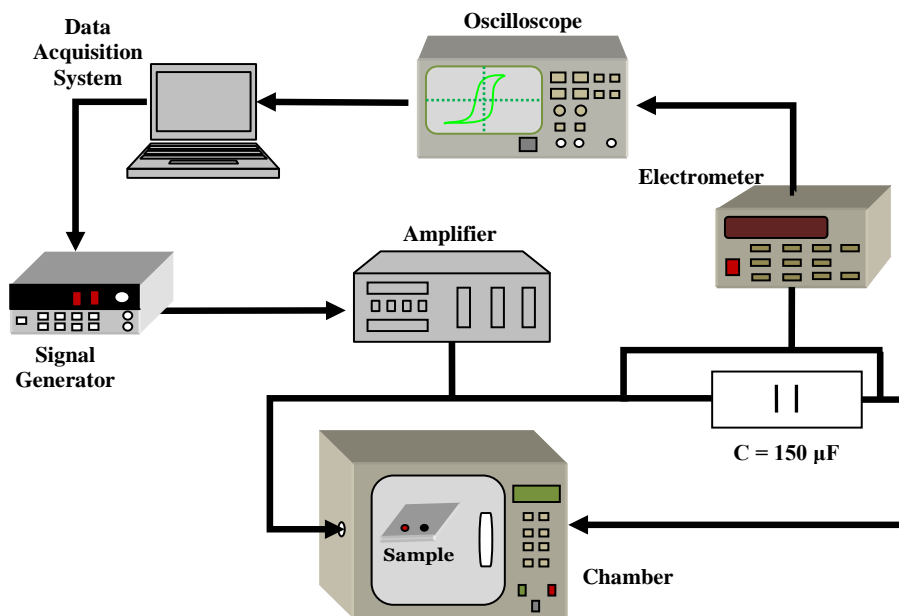
Figure 24 Sawyer Tower Set-up for experimental study of polarization vs. electric field (P-E) curves
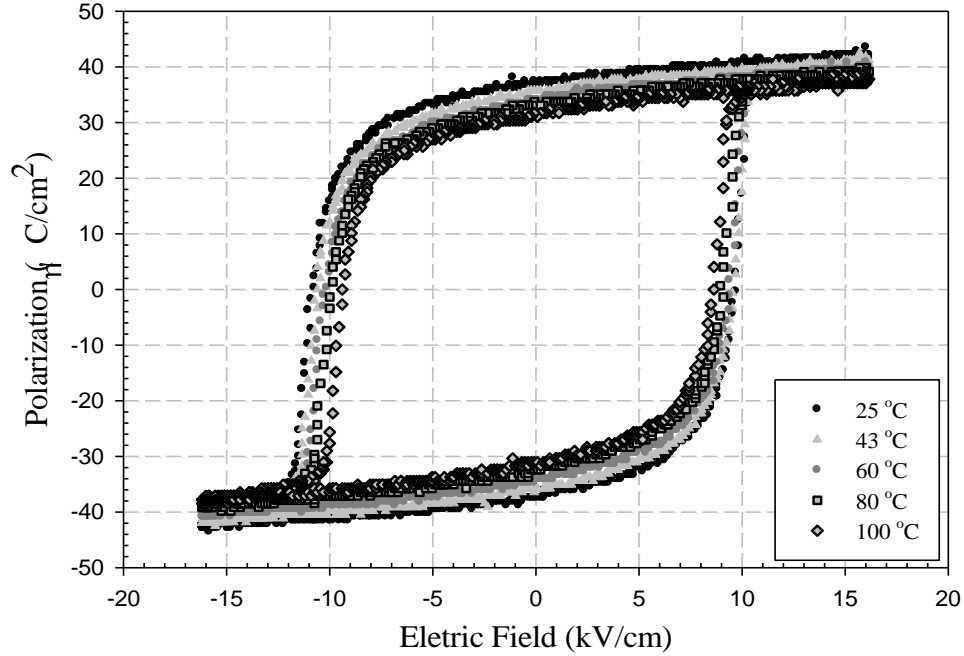
Figure 25 P-E curves measured at various temperatures

The pyroelectric coefficient of PZT is measured using the standard Sawyer Tower method. A drive signal is applied using an Aglient 33120A signal generator connected to a TREK model PZD2000 amplifier that produces quasistatic, cyclically varying field of large magnitude in the PZT. The polarization developed in the material due to the applied field can be estimated by the change in the electric displacement that leads to charge generation. This charge is measured by an electrometer connected to the sample through a bank of capacitors. The voltage signals indicative of the charge developed and voltage applied are recorded using an oscilloscope (Hewlett Packard model 54603B) and a National Instrument data acquisition system as shown in figure 24. This experiment is used to generate the hysteresis loop of polarization versus electric field. The intersection of the hysteresis loop and y-axis is remnant polarization (P_r), while the slope of this curve can be

used to estimate the relative permittivity near (P_r) or at zero field (Figure 24). By repeating this at different temperatures, variation of pyroelectric coefficient and relative permittivity with temperature can be obtained (Table 7).
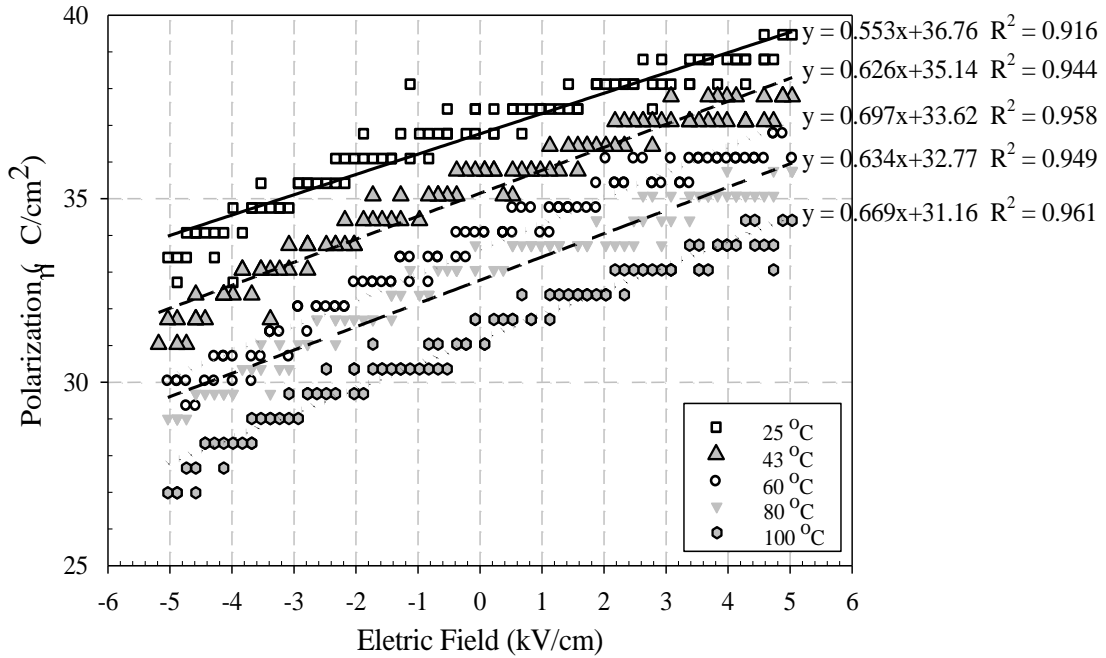
Figure 26 Remnant Polarization and Relative Permittivity at 22.5°C, 67.2°C and 102.2°C

The plot shows Polarization (C/cm^2) versus Electric Field (kV/cm) with the following fitted equations:

$y = 0.553x + 36.76$ $R^2 = 0.916$
$y = 0.626x + 35.14$ $R^2 = 0.944$
$y = 0.697x + 33.62$ $R^2 = 0.958$
$y = 0.634x + 32.77$ $R^2 = 0.949$
$y = 0.669x + 31.16$ $R^2 = 0.961$

Legend:
□ 25 °C
△ 43 °C
○ 60 °C
▽ 80 °C
⊗ 100 °C
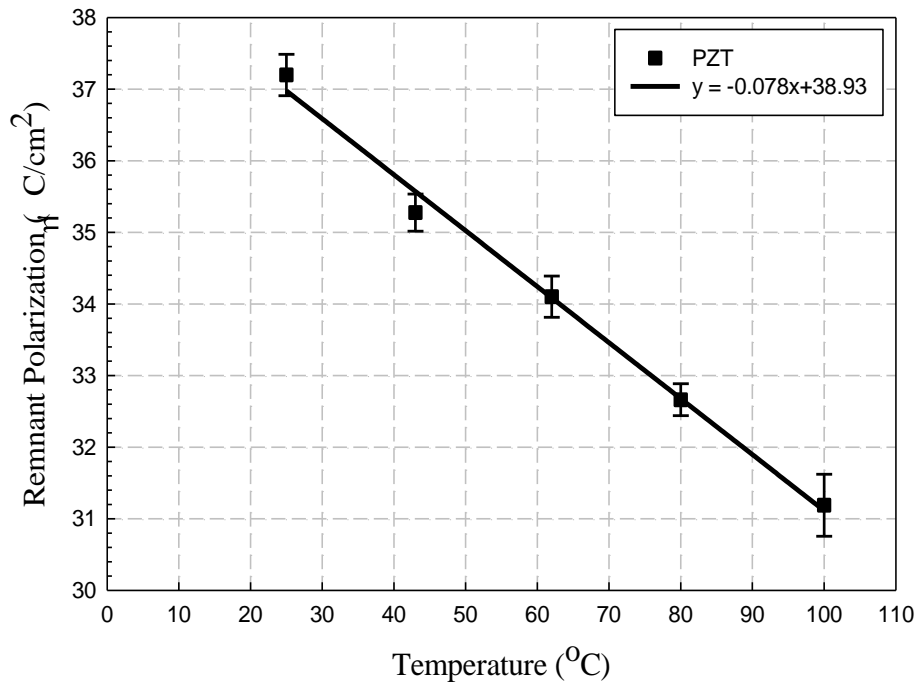
Figure 27 Determining the average pyroelectric coefficient

Table 7 Measured relative permeability (Espilon_R) and remnant polarization at 25°C, 43°C, 60°C, 80°C and 100°C. And Average pyroelectric coefficient over the entire temperature range.

Temperature (C)	Epsilon_R	Polarization (μCcm^{-2})	Avg Pyroelectric Coeff ($Cm^{-2}K^{-1}$)
25	6249	36.76	
43	7073	35.14	
60	7876	33.62	
80	7164	32.77	From Figure 22 (b)
100	7559	27.462	
Mean	**7184**		**780×10^{-6}**

The measurements at these limited temperatures show that the pyroelectric coefficient does not vary significantly with temperature. However, the relative

57

permeability at zero applied field varies by about 25% between 25°C and 100°C range, which affects the voltage developed across the pyroelectric samples for large changes in temperature.

<u>Scaling with Area</u>

The predicted voltage developed per unit temperature difference is independent of the area (equation 15). However, the experimental trends show an increase in voltage with surface area, which seems to level off at larger surface areas. This effect is especially pronounced with the 0.1 GΩ resistance (100% change in voltage from 200 mm^2 to 600 mm^2) but less pronounced for 10 GΩ (~ 10% change in voltage from While the analytical expressions predict the current, voltage, power and energy density for the pyroelectric material, only the voltage predictions are tested against experimental data. This is because the predicted voltage developed depends only on the temperature difference and not on the time history of the temperature variation. Thus if different regions of the sample heat at different rates, the voltage developed divided by difference between only the initial and final equilibrium temperatures (equation 15) provides good experimental data for comparison with model.

$$\frac{\Delta V}{\Delta T} = \frac{p'}{\varepsilon_0 \varepsilon_r} h \qquad \text{Equation 15}$$

The only parameters on which the voltage change per unit temperature difference depends are: the pyroelectric coefficient p' ($780 \times 10^{-6} \text{Cm}^{-2} \text{K}^{-1}$), ε_r (average estimated 7184) and thickness. The theoretical estimates are plotted with these values of parameters. Also a

58

revised estimate plots the voltage assuming p' ($255 \times 10^{-6} Cm^{-2}K^{-1}$), which is smaller but based on literature [Sebald et al., 2008] and ε_r of 4000.

The predicted voltage developed per unit temperature difference is independent of the area (equation 15). However, the experimental trends show an increase in voltage with surface area, which seems to level off at larger surface areas. This effect is especially pronounced with the 0.1 GΩ resistance (100% change in voltage from 200 mm^2 to 600 mm^2), but less pronounced for 10 GΩ ($\sim$ 10% change in voltage from 200 mm^2 to 600 mm^2).

Figure 28 Voltage/unit temperature difference at constant thickness=0.308mm. Blue straight line uses estimated parameters, red line uses revised parameters.

A possible reason for this is that as area increases the capacitance increases leading to higher RC time constant in Figure 28. This leads to less charge being lost due to current

flowing in the circuit, thereby producing a more accurate estimate of the voltage developed. But at high resistance values (for example 10 GΩ) the RC time constant is sufficiently high for even smaller areas and therefore the experiment matches theoretical trends more closely. For example the as area increased the experimentally measured capacitance increased from 14nF to 32nF. For R=0.1 GΩ, the RC time constant increases from 1.4s to 3.2s leading to larger voltage measured. For R=10 GΩ, the RC time constant increases from 140 s to 320 s leading to a more accurate measurement of the maximum voltage that can developed as the heating is performed over about 40s. Thus the voltage measurement with RC time constant of 320 s would be about 90% accurate. Future experiments are planned with higher resistance (500 GΩ to 1 Terra Ω) to ensure 99% accuracy.

Scaling with Thickness

The voltage increase with thickness matches the predicted trends for 10 GΩ, where as the 0.1 GΩ, shows significant deviations, possibly for reasons mentioned above.
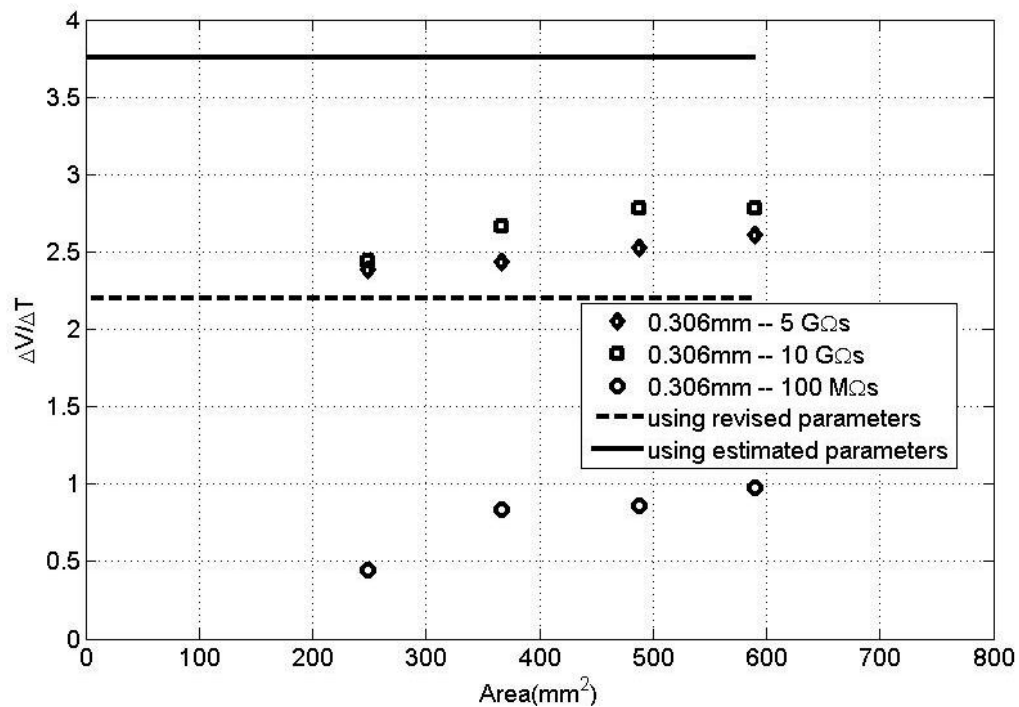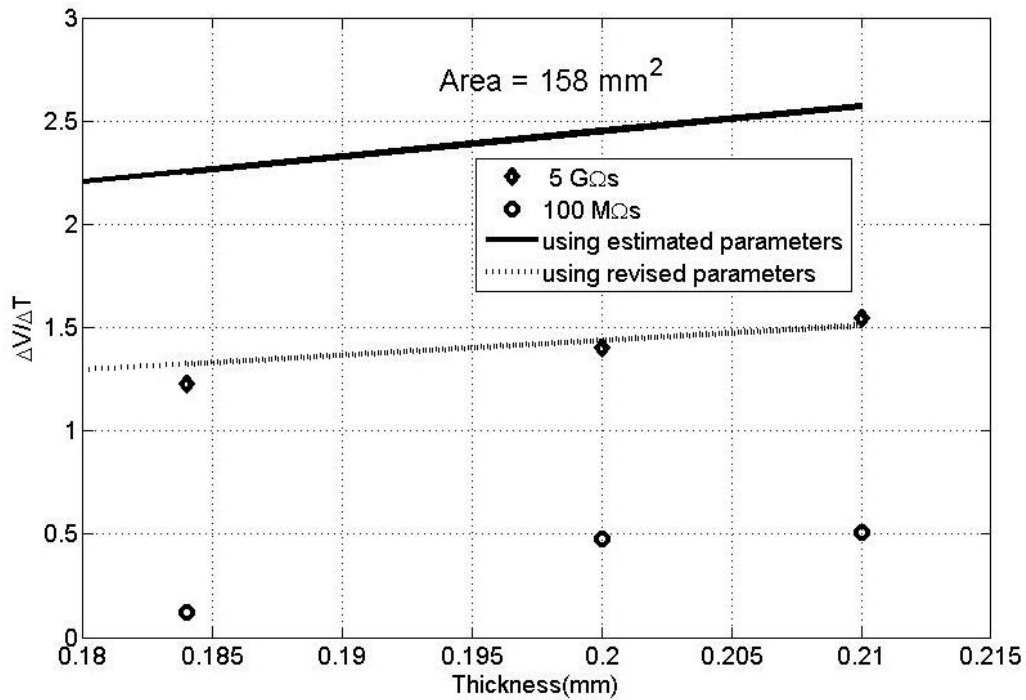
Figure 29 Voltage/unit temperature difference at constant area =158 mm^2. Blue straight line uses estimated parameters, red line uses revised parameters.

Another issue in comparison of both the thickness and area scaling data with analytical expressions is that the predicted voltages are about twice the values experimentally realized. These predictions are based on parameters p' and ε_r estimated from experimental P-E curves, which show a significantly larger p' (about 4 times) and larger ε_r that are typical for these materials. However, employing revised parameter values based on p' from prior literature (Xie, Mane, Mossi, & Leang, 2008) and lower ε_r make the voltages magnitudes match the experimentally measured voltage closer.

5.4 Sources of Error

The possible reason that the simulation results and experimental results are not always matching maybe due to the temperature gradient. This mismatch is documented through the Figure 30. These experiments were taken by an infrared camera Fluke Ti25. Temperatures are not uniform even on the same piece of the pyrolelectric materials as well as on the heater. In Figure 30(a), the maximum temperature on the pyroelectric materials (area A1) is 40.2 ˚C and the minimum temperature in area A1 is 28.4 ˚C at the same time. Figure 30(b) shows the temperature variation after heating is allowed to continue for a period of time. Similarly, the maximum temperature on the pyrorletric materials (area A1) is 73.9 ˚C and the minimum temperature in area A1 is 42.3˚C at the same time.

The frequency-domain model and the ideal model did not consider the heating transfer parameters. At a particular thickness the whole surface plate is not at the same temperature. The temperature measured using the thermocouple depends on the placing of the thermocouple. The thermal conductivity of the pyroelectric material does is not considered. Both of the models just consider the cooling behavior of the materials for convenience.
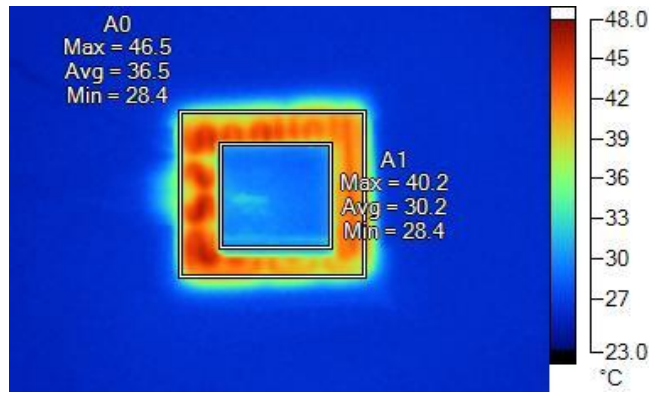
(a)
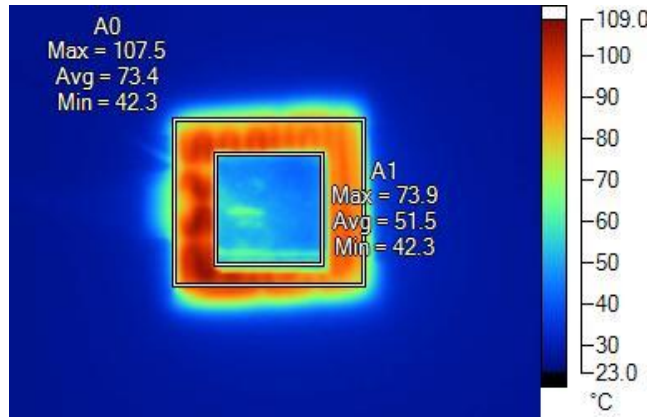
(b)

Figure 30 Temperature variations by infrared camera: (a) initial temperature variation
(b) temperature variation after heating a while

CHAPTER 6 Conclusions and Future Work

6.1 Static Heating System

In the pyroelectric energy harvesting via static heating, the potential for energy harvesting through the pyroelectric effect were studied by using piezoelectric materials such as PZT-5A, PMN-PT, and PVDF. A model was developed to predict the power generation. Measured results were compared to predicted results, as shown in Table 2. The measured results were in good agreement with the predicted results for the three tested samples. The results were within 4%, 8% and 9% for PMN-PT, PVDF, and PZT-5A, respectively. Peak power densities were experimentally determined to be $0.33\mu\mathrm{Wcm}^{-2}$, $0.20\mu\mathrm{Wcm}^{-2}$, and $0.12\mu\mathrm{Wcm}^{-2}$, for PMN-PT, PVDF, and PZT-5A, respectively. Using the model it was predicted that a thin-film with large area and significantly higher pyroelectric coefficient can generate nearly three orders of magnitude improved peak power density under similar boundary conditions as the PZT-5A, PMN-PT, and PVDF samples.

6.2 Cyclic Heating System

For continuous energy harvesting using PZT, a prestressed PZT composite and single crystal PMN-30PT single crystal elements were utilized. These materials were selected for their properties, easy of availability and enhanced properties. A cyclic heating

system is designed which periodically heats and cools the pyroelectric elements creating periodic temperature gradients. As a benchmark for traditional methods a static heating system is also tested using typical parameters which are not optimal. With the cyclic system the temperature gradients and consequently the power generation is also smaller. It is also observed that higher power densities were generated at low frequency heating due to high temperature gradients that can be achieved during these periods. The impedance matching resistance in the power measurement circuit is optimized to 8MΩ for the PZT samples. The peak power densities were generated with PMN-30PT single crystals at 8.64μW/cm^3. The energy harvested by prestressed PZT composites was 40% larger than with simple PZT ceramics. The measured coefficient of PZT composite is two times larger than PZT, indicating enhanced performance. Further testing is required to clearly determine the effect of pre-stress on the power generation.

6.3 Analytical Expressions for Ideal Power

Simple analytical expressions are developed for ideal voltage, power and power densities as a function of pyroelectric constant, permittivity, surface area, thickness, temperature variation and rate of change for unclamped samples. The experimental trends of scaling with the area show a pronounced increase with the 0.1 GΩ resistance (100% change in voltage from 200 mm^2 to 600 mm^2). But less pronounced for 10 GΩ (~ 10% change in voltage from 200 mm^2 to 600 mm^2). In the scaling with thickness, the voltage increase with thickness matches the predicted trends for 10 GΩ. The predicted trends (not magnitudes) for voltage developed as for varying thickness and area match experimental

65

observations. However, it was found that it is crucial to use sufficiently high resistances to limit the flow of current (or loss of charge) in the measurement circuit, which is one of the causes for deviation from predicted voltages. Secondly, model parameters estimated from experimental P-E data appeared larger than that reported in literature. This is likely to be another reason for larger magnitudes of voltage predicted than actually measured. A larger set of experimental data generated from tests employing higher resistance values for the measuring circuit need to be performed to further validate these expressions and use them as a tool for estimating the maximum theoretical power that can be harvested from pyroelectric devices.

6.4 Further Work

The potential for energy harvesting through the pyroelectric effect was demonstrated numerically and experimentally. One avenue to enhance energy generation is to use pyroelectric materials with significantly higher pyroelectric coefficients. Another one is to maximize the surface area. Some representative papers from literature are mentioned that various parameters affect pyroelectric properties of thin film. The thin film with large area and significantly higher pyroelectric coefficient can be used in the experiments to according to the model prediction. In addition, earlier studies [Mossi *et al*., 2005] show that the effective piezoelectric coefficient of pre-stress composite might be one or two order larger after pre-stressed. Due to the enhanced strain capabilities, it shows the possibility that enhanced performance of energy harvesting materials is possible by pre-stress. From the model prediction, it shows the power generation by thin film with large

66

area performed satisfactorily. One of the major applications of energy harvesting is to power the portable electronics. Piezoelectric and pyroelectric effect could be combined in the energy harvesting in an effect to harvest enough energy to power another system.

References

APC International, Ltd., 2002. "Piezoelectric Ceramics: Properties & Applications". Mackeyville, Pennsylvania.

Antaki, J., Bertocci, G., Green, E., Nadeem, A., Rintoul, T., Kormos, R. and Griffith, B. 1995. ''A Gait Powered Autologous Battery Charging System for Artificial Organs,'' ASAIO Journal, 41:M588–M595.

Baert, K., Gysellinckx, B., Torfs, T., Leonov, V., Yazicioglu, F., Brebels, S.,Donnay, S., Vanfleteren, J., Beyne, E. and Van Hoof, C., 2006. "Technologies for highly miniaturized autonomous sensor networks." *Microelectronics Journal,* vol. 37(12), pp.1536-1568.

Clingman, W. H., and Moore, R. G., 1961. "Application of ferroelectricity to energy conversion processes," *Journal of Applied Physics,* vol. 32, p. 675.

Cuadras, A., Gasulla, M., Ghisla, A., and Ferrari, V., 2006. "Energy harvesting from PZT pyroelectric cells," In Instrumentation and Measurement Technology Conference, Sorrento, Italy, pp. 1688 – 1672.

Guyomar, D., Sebald, G., Lefeuvre, E., and Khodayari, A., 2009. "Toward heat energy harvesting using pyroelectric material," *Journal of Intelligent Material System and Structures,* vol. 20, pp. 265–271.

Kymissis, J., Kendall, C., Paradiso, J. and Gershenfeld, N. 1998. ''Parasitic Power Harvesting in Shoes,'' In: Second IEEE International Conference on Wearable Computing (ISWC), IEEE Computer Society Press, pp. 132–139.

Lefeuvre, E., Badel, A., Richard, C. and Guyomar, D., 2005"Piezoelectric Energy Harvesting Device Optimization by Synchronous Electric Charge Extraction," *Journal of Intelligent Material Systems and Structures,* vol. 16, p. 865.

Malmonge, L. F., Malmonge, J. A., and Sakamoto, W. K., 2003. "Study of pyroelectric activity of PZT/ PVDF-HFP composite," *Materials Research,* **6**(4), pp469 – 473.

Mossi, K., Selby, G., and Bryant, R., 1998. "Thin-layer composite unimorph ferroelectric driver and sensor properties," *Material Letters,* vol. 35.

Mossi, K., Bishop, R., Smith, R. and Banks, J., 1999. "Evaluation Criteria for THUNDER Actuators," in *SPIE-The International Society for Optical Engineering*, pp. 738-743.

Mossi, K., Green, C., Qunaies, Z., and Hughes, E. (2005). "Harvesting energy using a thin

unimorph prestressed bender: Geometrical effects." Journal of Intelligent Material Systems

and Structures, 16(2), 249 – 261.

Olsen, R. B., Bruno, D. A., and Briscoe, D. A., "Pyroelectric conversion cycles," *Journal of Applied Physics,* vol. 58, p. 4709, 1985b.

Ottman, G., Hoffman, H., Bhatt, A. and Lesieutre, G. 2002. ''Adaptive Piezoelectric Energy Harvesting Circuit for Wireless Remote Power Supply,'' IEEE Transactions On Power Electronics, 17(5):669–676.

Ottman, G., Hoffman and Lesieutre, G. 2003. ''Optimized Piezoelectric Energy Harvesting Circuit Using Step-Down Convertor in Discontinuous Conduction Mode,'' IEEE, 18(2):696–703.

Paradiso, J. A. and Feldmeier, M., 2001. "A compact, wireless, self-powerered pushbutton controller," in *Ubicop.*

Paradiso, J.A., and Starner, T., 2005. "Energy scavenging for mobile and wireless electronics," *Pervasive Computing,* January – March, pp. 18 – 27.

Roundy, S. 2003. "Energy Scavenging for Wireless Sensor Nodes with a Focus on Virbarion to Electricity Conversion."

Roundy, S., Wright, P., and Rabaey, J., 2004. *Energy Scavenging For Wireless Sensor Networks*. New York, NY: Kluwer Academic Publishers.

Rowe, D.M. 1995. CRC *Handbook of Thermoelectrics*, CRC Press, Boca Raton, FL.

Rowe, D.M. 1999. "Thermoelectric, an Environmentally-Friendly Source of Electricl Power," *Renewable Energy*, 16(1):1251.

Sebald, G., Seveyrat, L., Guyomar, D., Lebrun, L., Guiffard, B. and Pruvost, S., 2006. "Electrocaloric and pyroelectric properties of 0.75Pb ($Mg_{1/3}$ $Nb_{2/3}$) O_3-0.25$PbTiO_3$ single crystals," *Journal of Applied Physics,* vol. 100, p. 124112.

Sebald, G., Lefeuvre, E., and Guyomar, D., 2008. "Pyroeectric energy conversion: optimization principle," *IEEE Trans Utransonic, Ferroelectrics and Frency Cont.,* 55(3), pp538-551.

Shenck N. S. and Paradiso, J. A., 2001. "Energy scaving with shoe-mounted piezoelectrics," *IEEE Micro,* vol. 21, pp. 30–42.

Sodano, N. S., Park, G., Leo., and Inman, D. J., 2003. "Use of piezoelectric energy

harvesting devices for charging batteries," *Proceedings of the SPIE – The international Society for Optical Engineering*, 5050, 101-108.

Sodano, H., Lloyd, J. and Inman, D. 2004. ''An Experimental Comparison Between Several Active Composite Actuators For Power Generation,'' Proc. SPIE Int. Soc. Opt. Eng., 5390:370–378.

Ujihara, M., Carman, G. P., and Lee, D. G., 2007. "Thermal energy harvesting device using ferromagnetic materials," *Applied Physics Letters,* **91,** p. 093508.

Whatmore, R.W., 1986. "Pyroelectric devices and materials," *Rep. Prog. Phys.,* **49,** pp, 1335 – 1386.

Wise, S., 1998. "Displacement properties of Rainbow and Thunder piezoelectric actuators," *Sensors and Actuators A,* vol. 69, pp. 33–38.

Zhang, J., Hladky-Hennion, A., W. Hughes, W., and Newnham, R., 2001. "Modeling and underwater characterization of cymbal transducers and arrays," *IEEE Transactions on Ultrasonics, Ferroelectrics, and Frequency Control,* vol. 48, pp. 560–568.

APPENDIX A

This Chapter presents the Matlab code for the power generation of the model based on the static heating approach. In addition, the measured and predicted power measurements are compared.

```matlab
% HOTT Project

% Power measurement using resistor and AD549 op-amp

clear all


t = (1/1000)*[0:29999]';


t01 = load('t01m.out');      % R=1 MOhm

V01 = t01(60001:90000);

T01 = t01(30001:60000);


% R = 1.0 Mohm

% ====================================================================

% Measured power using V(t)

P01m = V01.^2/1e6;


% Predicted power using T(t)

% Area of PZT

Area = 0.012^2;          % m^2 area of piezoelectric materials

py = 238e-6;             % uC/m^2K pyroelectric coefficient of piezoelectric

                          materials
```

```matlab
Cp = 45e-9;            % capacitance of piezoelectric materials

Re = 1e6;              % external resistance


% filter temp data

[B,A] = butter(5,.005);

Tf01 = filtfilt(B,A,T01-T01(1)) + T01(1);  % filtered temp

dT01 = gradient(Tf01)*1000;


% Voltage model

G = tf([py*Area 0],[C 1/Re]);


% Predicted output voltage, Vp

[Vp,t] = lsim(G,Tf01-Tf01(1),t);

P01p = Vp.^2/Re;  % predicted power


figure(1); clf;

subplot(311);

plotyy(t,T01,t,dT01);

subplot(312);

plot(t,V01,'k',t,Vp,'r--'); xlabel('Time (s)'); ylabel('Voltage');

subplot(313);

plot(t,P01m*1e6,'k',t,P01p*1e6,'r--'); xlabel('Time (s)'); ylabel('Power

(\muW)');


m(:,1)=t;

m(:,2)=T01;
```

```matlab
m(:,3)=dT01;

m(:,4)=t;

m(:,5)=V01;

m(:,6)=Vp;

m(:,7)=t;

m(:,8)=P01m*1e6;

m(:,9)=P01p*1e6;

xlswrite('PZT_JIM', m);
```

APPENDIX B

This Chapter presents the Matlab code for the power generation of the model based on the cyclic heating approach. In addition, the code include the Savitzky-Golay filter which used for filter the temperature signals

```
clear all
t=load('C:\Documents and Settings\shubham\Desktop\timecyclic.txt');
temp=load('C:\Documents and
Settings\shubham\Desktop\temperaturecyclic.txt');
pd=load('C:\Documents and Settings\shubham\Desktop\powercyclic.txt');
pm=26.754e-3*pd;                         % power = volume* power density
sm =sgolayfilt(temp,6,201);            % Savitzky-Golay filter of order 6
dT=gradient(temp)/diff(t);
dT2=gradient(sm)/diff(t);                                %Area of PZT
area=98e-6;                                                    %m^2
py=416e-6;   % pyroelectric coefficient
cp=17.4e-9;  % capacitance value
ce=0;    % external capacitance
c=ce + cp;
re=7e6;    %resistance value
vol= load ('C:\Documents and Settings\shubham\Desktop\PMNPT.txt')
%formulation of transfer function
trans = tf([py*area 0],[c 1/re]);
[vp2,t] = lsim(trans,sm-sm(1),t);
p1=(vp2).^2/re;       %predicted power
```

```
figure(1); clf;

subplot(221);

plot(t,temp,'r');grid on; xlabel('Time (s)'); ylabel('Temperature');

subplot(222);

plot(t,sm);grid on;xlabel('Time (s)'); ylabel('Temperature');

subplot(223);

plot(t,dT);grid on;xlabel('Time (s)'); ylabel('dT/dt');

subplot(224);

plot(t,dT2);grid on;xlabel('Time (s)'); ylabel('dT/dt');

energym=trapz(t,pm)

energyp=trapz(t,p1*1e6)

error= ((energyp-energym)/energym)*100

figure(2);clf;

plot(t,vol,'r',t,(vp2),'g');grid on;xlabel('Time (s)'); ylabel('Voltage
(volts)');

legend('measured voltage','predicted voltage');

figure(3);clf;

plot(t,pm,'k',t,p1*1e6,'r--'); xlabel('Time (s)'); ylabel('Power
(\muW)');

legend('measured power','predicted power');
```

VITA

Jingsi Xie was born in Chongqing, P.R. China on 5th of February in 1985. She was raised in the Chongqing and graduated from Bashu High School in August of 2007. Following her high school, Ms. Xie attended the Southwest Jiaotong University in China where she obtained a Bachelor of Science in Electrical Engineering in August 2007. While pursuing her undergraduate degree, she was awarded the Engineering Scholarship for outstanding study.

Ms. Xie went to pursue her graduate degree at Virginia Commonwealth University, where she received the Dean's fellowship and full financial support as research assistant. While pursuing her Master's as the research assistant in Smart material Lab, Jingsi has co-authored works have been published in *Smart Materials and structures* and has presented findings at the conference for the SPIE's International Society for Optic Engineering, in 2009, as well as the ASME conference, held in Ellicot City, MD, 2008.